A 3 DOF Pneumatic Manipulandum for Wrist Rehabilitation

By

Yasser Aleed

A Thesis submitted to the Faculty of Graduate Studies in

partial fulfillment of the requirements for the degree of

Master of Science

Department of Mechanical Engineering

Faculty of Engineering

University of Manitoba

Winnipeg, Manitoba, Canada

September 2020

Abstract

Robotic assistive technologies are increasingly used to enhance the physical rehabilitation of patients who have suffered disorders such as strokes. Not only does it make the lives of disabled and elderly patients easier, but it also improves their body functionalities. Robotic assistive technologies offer people a second chance to overcome challenges that come with their disability.

The objective of the thesis is to design, prototype and evaluate a 3 Degrees of Freedom (DOF) pneumatic manipulandum for wrist rehabilitation that is capable of accommodating to wrist motions (ulnar deviation, radial deviation, flexion or extension). Since the wrist is the most mobile part of the hand, its post-stroke rehabilitation is difficult. In order to accommodate the wrist motion, 3 DOF are needed. 2 DOF are needed for the horizontal motion and another DOF to allow the manipulandum to move up and down with the wrist. Each DOF is actuated by one pneumatic actuator. The design is prototyped using a 3D printer. The workspace and the required force are analyzed and calculated based on the kinematics of the manipulandum. The pneumatic actuators that were chosen are available in non-magnetic material, which means they are compatible with Functional Magnetic Resonance Imaging (fMRI-compatible).

The manipulandum is connected to a Neuro Function Evaluation (NFE) game which is used in the Rehabilitation Centre in Winnipeg. While running the game, the manipulandum is tested and evaluated in assistive and resistive modes. The performance of the manipulandum is analyzed using two methods: image processing and file streaming. The image processing method determines the location of the ball and the location of the paddle of the NFE game in the screen by taking screenshots, while the file streaming method is used to obtain those two locations from the code of the game itself.

Acknowledgments

In the name of Allah, the Most Beneficent, the Most Merciful.

First and foremost, all praises and thanks to Allah, the Almighty. I could not have completed this thesis without His countless favors and blessings.

I owe the deepest gratitude to my research supervisor Dr. Nariman Sepehri. His knowledge, experience and kindness helped me a lot during my master's program. It has been an honor for me to work under his supervisions.

I would like to thank my friends, Dr. Khurram Butt, Dr. Ali Maddahi, Dr. Ehsan Jalayeri, and Dr. Guangan Ren for their support during my research.

No words can describe my deep sincere thanks to my grandmother Khadeja, my parents, Hassan Aleed and Hiam Hamada, my wife Rouaa Al Thair, my cousin Ahmad Aleed, my brothers and sisters.

Finally, I would like to place on record my gratitude for all those who directly or indirectly lent their hand in this venture.

Dedication

I dedicate this thesis to my grandmother Khadeja, my parents, Hassan Aleed and Hiam Hamada,

who brought me up with unconditional love and sacrificed their own needs for my education and

well-being. To my wife Rouaa Al Thair, you have been an inspiration. Thank you for your support

and encouragement, every day, even from afar. It has always made a difference

Table of Contents

List of Figures

List of Tables

1. Introduction

1.1. Statement of the problem

According to the World Health Organization (WHO) in 2007, "neurological disorders due to epilepsy, Alzheimer's disease or stroke affect up to one billion people worldwide. In addition, one of the most common disabilities that patients face after having a stroke is paralysis, which affects the body's motor functions. For instance, stroke patients with either hemiplegia (one-sided paralysis) or hemiparesis (one-sided weakness) face many difficulties in everyday activities like walking or grasping objects" [1]. Patients often face severe financial difficulties when accessing appropriate care. On a global scale, the annual burden caused by strokes is about $65.5 billion, which makes post-stroke rehabilitation a critical issue [2].

Primary health care is the only medical care available to many patients seeking recovery after experiencing a stroke. In these settings, health care providers traditionally rely on physical repetitive exercises. Although these exercises have been used to great success for many people, they do have their shortcomings. The repetitive nature of physiotherapy can be dull, and patients may not work as diligently as instructed. Additionally, the repetitive nature of physiotherapy can make it difficult to provide quantitative measures to track progress. An innovative alternative form of treatment which is not only effective and low-cost but also more engaging and provides direct measurements of progress is robot-assisted technologies such as manipulandums or haptic devices [3]. Additional benefits of robot-assisted treatment include increasing the duration of treatment sessions while allowing it to be more intensive [4]. Robot-assisted technologies are capable of providing these benefits by turning the treatment process into motivating tasks such as games. Haptic devices can be interfaced with a virtual game which transforms the treatment process into something that is stimulating and exciting as well as provides a quantitative means to track a

patient's rehabilitation progress. These quantitative measures allow physicians to better support and ensure ideal conditions for motor learning and recovery of function.

Haptic devices are one form of robot-assisted technologies. They can include steering wheels, finger pads, robotic handles, grippers, joysticks, or gloves [5]. When a patient moves the joint of a haptic device, the haptic device reacts by applying force feedback. In other words, the input of a haptic device is the user's movements and the output is the force feedback. These movements of the device are what is tracked digitally and can be mapped directly into a game space in which the game is controlled directly though the patient's rehabilitation exercise. Depending on the desired goal, the force feedback could be programmed to assist or apply resistance to the patient's movements.

Magnetic Resonance Imaging (MRI) is a common tool used by health care providers to assess the progress of treatment. It is a non-invasive imaging technology that produces three-dimensional detailed anatomical images without the use of damaging radiation. MRIs employ powerful magnets that produce a strong magnetic field to produce their images [6]. For this reason, it is essential that the device's material composition does not contain any metal that could distort these images [7]

Robot assisted devices can be utilized for stroke patient to great effect, in particular in the rehabilitation of the wrist. The function of the wrist joint is to provide a range of motion necessary to adequately perform daily functions while maintaining a physiologic level of inherent stability. This movement allows for a wide range of motion necessary to facilitate the functional use of the hand [8]. Compared to the rest of the arm, the rehabilitation of a non-functional wrist is difficult. If the wrist is not functional, the hand's function is compromised. Consequently, if the hand is not functional, the arm's function is compromised.

1.2.   Objectives

The primary objective of this thesis is to design and construct a prototype manipulandum that has the following characteristics:

(i)   Is cost-effective to a point where it can be widely implemented as an alternative form of treatment.

(ii)   Provides force-feedback that is capable of accommodating movement of the wrist in two direction.

(iii)   Provides a platform that is capable of both assisting and applying resistance to the motions of the wrist.

(iv)   Is available in fMRI-compatible material to support fMRI studies.

1.3.   Scope of the thesis

This thesis recognizes the difficulties in rehabilitating the wrist and offers a way to design a pneumatically actuated manipulandum for wrist rehabilitation. It first provides a historical background on the use of manipulandum as rehabilitation devices, including a description of various mechanical designs of devices. A thorough overview of relevant previous work is provided as a foundation for the design of a new device. The detailed analysis of the manipulandum includes the consideration of mechanical design and workspace parameters, material selection, hardware choices such as actuators and sensors, and controller design. The device adopted a Neuro Function Evaluation (NFE) game as a focus of analysis for this thesis. The game is used in the Rehabilitation Centre in Winnipeg. The game was tested using three modes: assistive mode, resistive mode and assistive with hysteresis mode. These three modes analyzed the performance of the manipulandum

and provided quantitative measures and an in-depth discussion about the successes and shortcomings of the device.

2. Background

According to the Oxford dictionary, *haptic* refers to the sense of touch, which relates to the perception and manipulation of objects using the senses of touch and proprioception. The word derives from the Greek "haptikos" which means "being able to come into contact with" [9]. Haptic technology is the science of touch. Haptic devices have been extensively investigated and applied in many fields, such as teleoperation, robotic surgery, bioengineering, and computer-aided design [10]. Haptic devices are designed based on their application. They usually have multiple Degrees of Freedom (DOF). For example, haptic devices with 6-DOF may have the best performance because the human hand is capable of sensing all the possible 6-DOFs in 3D space. Depending on the sequence of links and joints, haptic devices are divided into serial, parallel, or hybrid, which is a mix of both serial and parallel. A manipulandum is a robot that provides force feedback to the user. Under the definition provided a manipulandum is a form of haptic device.

2.1. Historical review

Force feedback devices are the first haptic interfaces that were used for teleoperation in Robotics (1950s-1980s). In 1954, Raymond Goertz, working in Argonne National Laboratories, used force feedback devices in a robotic teleoperation system for nuclear environments. In 1993, the commercial force feedback devices appeared, notably the PHANTOM arm, the Impulse Engine in 1995 and the CyberGrasp glove in 1998. Development started on the touch feedback devices in 1990, including the Dexterous Hand Master Exoskeleton which produced vibrations on the user's fingertips, and the Sandpaper Tactile Joystick which mapped image texels (texture elements) to vibrations [11].

The first manipulandum, built in the University of Western Ontario, was described as a device for accurate measurements of elbow movements (see Figure 2-1) [12] [13] [14]. Its design allowed for repeated tests of human motor performance which comprised of moving a handle under diverse imposed conditions. This manipulandum was effectively used as a tool to analyze the movement parameters of patients diagnosed with Parkinsonism or cerebellar disease. The accuracy of this manipulandum was limited. For example, the amount of "inertial compensation" that can be added to the torque command signal is limited by the mechanical resonance of the handle/housing.

Tachometer (A)

Torque motor (B)

Clamps (C, F).

Pitch(D), Roll (F)

U-support (E),

Handle (G)

Grasps a knob (H)

Arm rest (I)

Mechanical stops (K).

Chair (L)

Massive stand (M),

Lockable positions (N)

Rails (O)
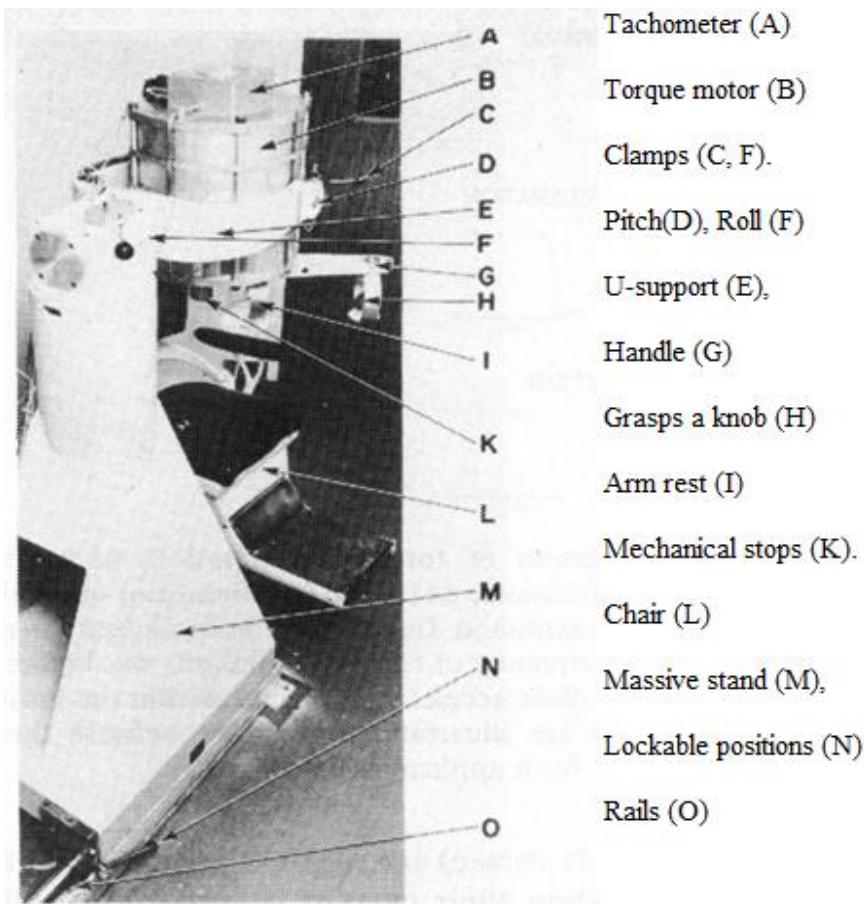
Figure 2-1. View of manipulandum for human motor studies (source [12])

The patient sits in the chair (L), his/her arm rests on the arm rest (I) and grasps a knob (H) to stabilize the hand. Excursion of the handle is limited by mechanical stops (K).

In 1990 Walter Gezari and Daniel Y. Gezari designed a manipulandum which they called a muscle exercise and/or rehabilitation apparatus (see Figure 2-2). This device was used for evaluating the performance of the entire body during lifting with respect to work fitness and disability [13].
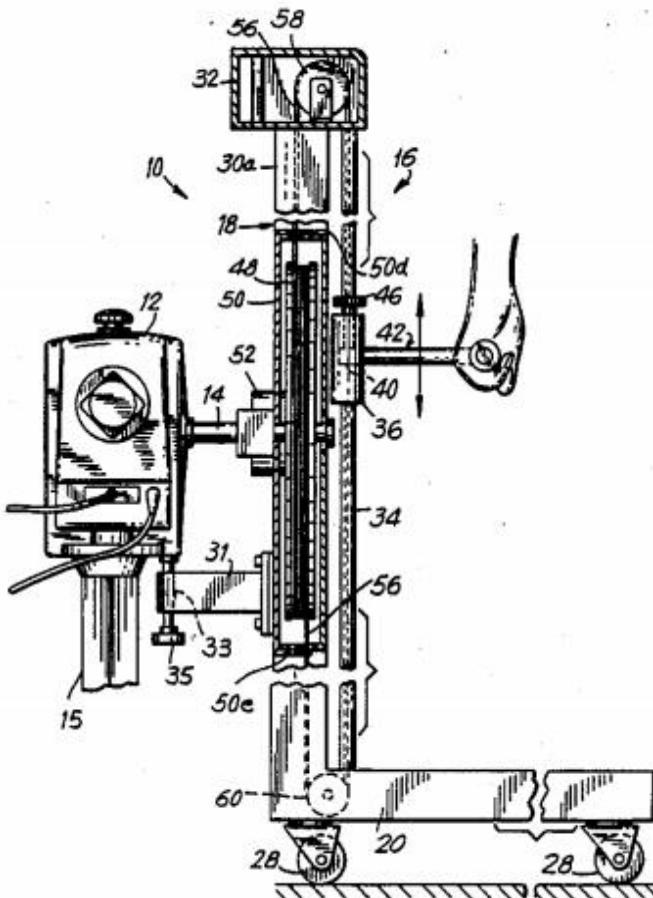
Figure 2-2. Muscle exercise and/or rehabilitation apparatus (source [13])

An MRI compatible manipulandum actuated by the ultrasonic motors was developed [14], which was able to work within the MRI scanner and perform fMRI tasks continuously during finger movements (shown in Figure 2-3).

(1) The manipulandum

(2) Driver system

(3) and (4) Power supply

(5) RT-Linux PC
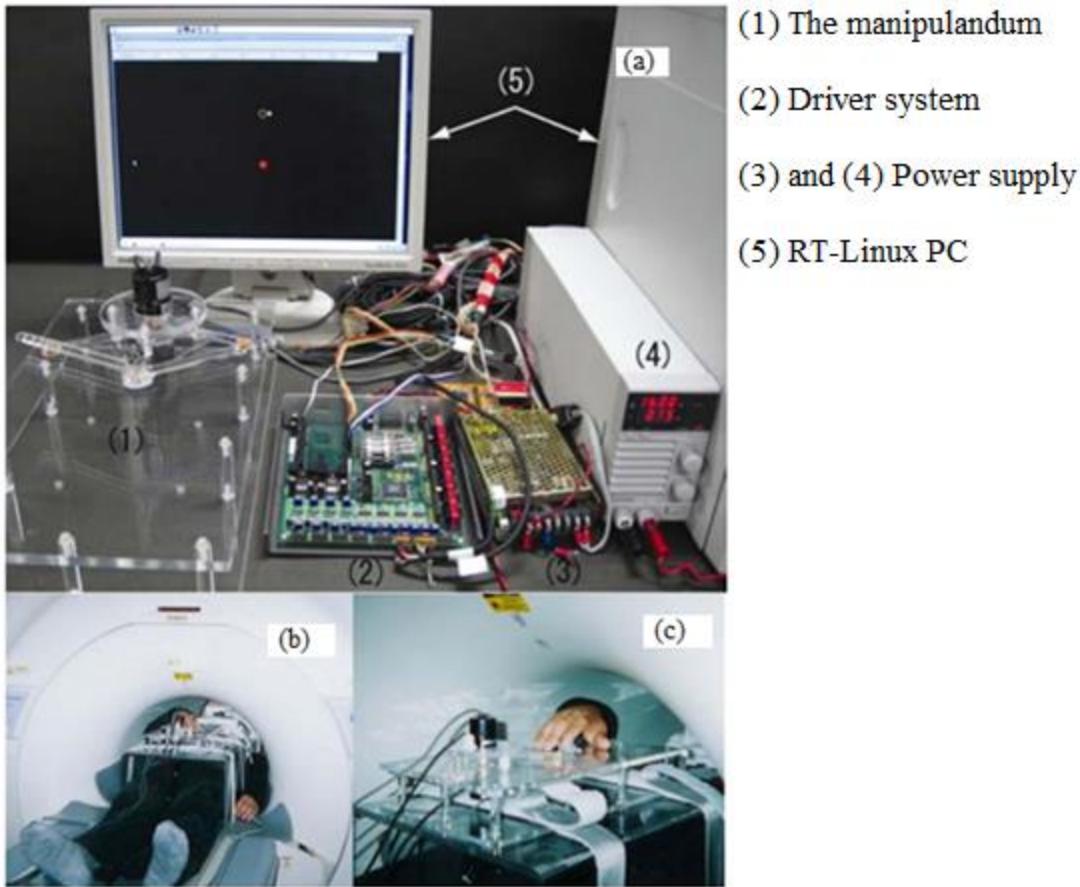
Figure 2-3. (a) Overview of manipulandum, (b) and (c) manipulandum with MRI scanner (source [14])

A haptic device (manipulandum) was developed for upper extremities and to evaluate the muscle's efficacy in upper limb muscle activities (see Figure 2-4) [15]. Moving the grip of the device provides a virtual force to the user, either assisting the movement of their arm or acting as a resistive force against it.
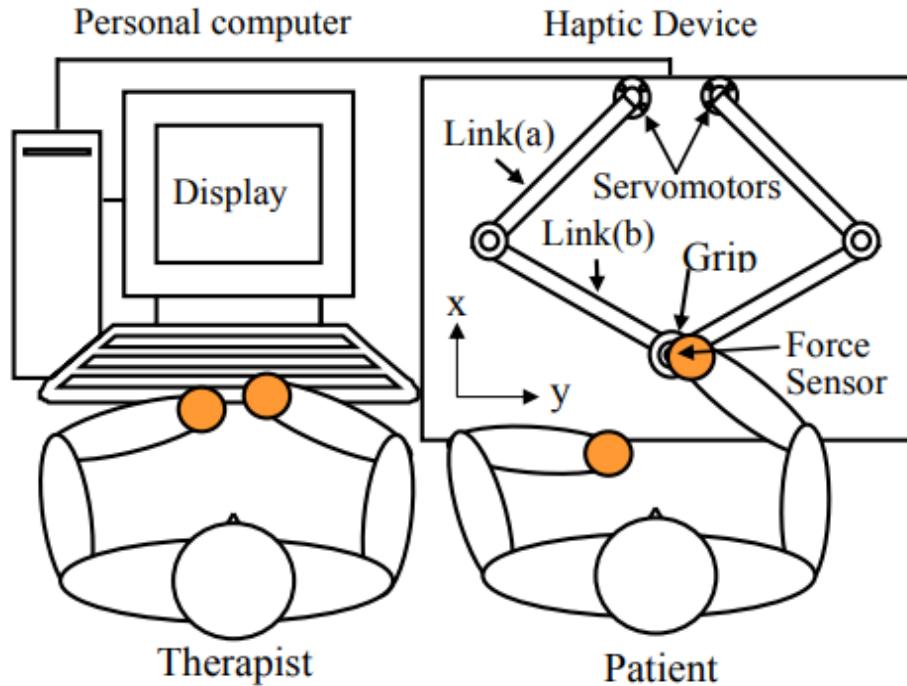
Figure 2-4. Haptic device system for upper limb rehabilitation (source [15])

All of the above-mentioned examples provide proof of concept to the advent of robots becoming a popular means of rehabilitation since they can provide well-controlled repeatable tasks with manageable costs [16].

The design of a manipulandum depends on its future application or use. A variety of mechanisms can be utilized in configurations which are classified as serial, parallel or hybrid. Serial kinematic machines have already reached their dynamic performance limits of having high stiffness due to the machine components required to support sequential joints. Parallel kinematic machines have many advantages over serial configurations, including higher rigidity, payload-to-weight ratio, higher accuracy, and the possibility of locating actuators on the fixed base. These advantages allow parallel-kinematic manipulators to reach higher dynamic capabilities than serial [17]. Parallel-kinematic manipulators have been employed in many instances as haptic device mechanisms [18],

9

[19], [20], [21], [22] and [23]. One of the most famous parallel-type haptic devices is the Delta haptics [24], [25], [26], and [27].

The main advantage of hybrid serial-parallel structures such as the device presented in [28], is that it reduces the inertia of the device and allows the use of high power (and heavy) motors. The electromechanical manipulandum for upper limb rehabilitation (EMU) (shown in Figure 2-5) was designed to help to rehabilitate the upper limbs of patients with neurological motor impairments. The device has a large enough workspace to cover the range of motion of healthy patients. However, the dynamics of the EMU have a weak impact on the resulting movements made with the arm.

Figure 2-5. EMU prototype with a subject (Source: [29])

2.2. Summary

This chapter firstly provided a historical overview of previously developed manipulandums, which each served various rehabilitation purposes. This chapter secondly provided an overview of the limits and specifications of each form of machine (parallel, series and hybrid). However, the haptic devices introduced in this chapter do not provide solutions to the problems that this thesis is addressing. The key problems are that they are not of small size, they do not possess high force, they are not pneumatically actuated, and they are not available from a non-magnetic material.

3. Prototypes Previously Developed

This chapter will discuss various prototypes that were previously developed in the Fluid Power and Telerobotics Research Laboratory at the University of Manitoba. These prototypes will be analysed and evaluated in the XY plane, because the NFE game adopted by this thesis is a 2D game that has a paddle moving in X direction and a ball falling in Y direction.

3.1. First prototype

This robot was designed to evaluate the performance of the designed mechanisms. The first manipulandum design provided 6 DOF (see Figure 3-1). The robot was built from aluminum. The first joint was prismatic and defined the Z position of the end-effector, which made the positioning controller easier to design and implement. The second and third joints were revolute. Both joints were parallel to each other and rotated around the Z axis (2nd joint rotate around Z_1 and 3rd joint rotate around Z_2). The next three revolute joints were designed to generate the required orientation for the end-effector. A parallel structure was used to keep the end-effector in a certain position with respect to the third joint. The main idea for this structure was proposed to decouple the end-effector's positions and orientations.

Figure 3-2 shows the CAD model of the first 3 DOF manipulandum, including the location of the joints and the location of the actuators. The CAD model will be used to extract the kinematics of the manipulandum.
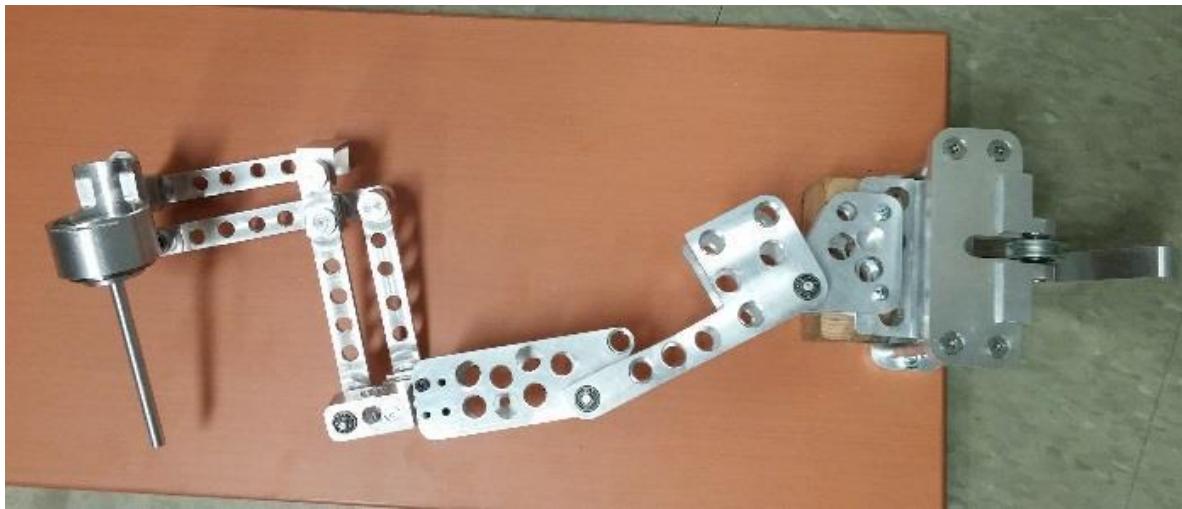
Figure 3-1. First prototype device (source [30])
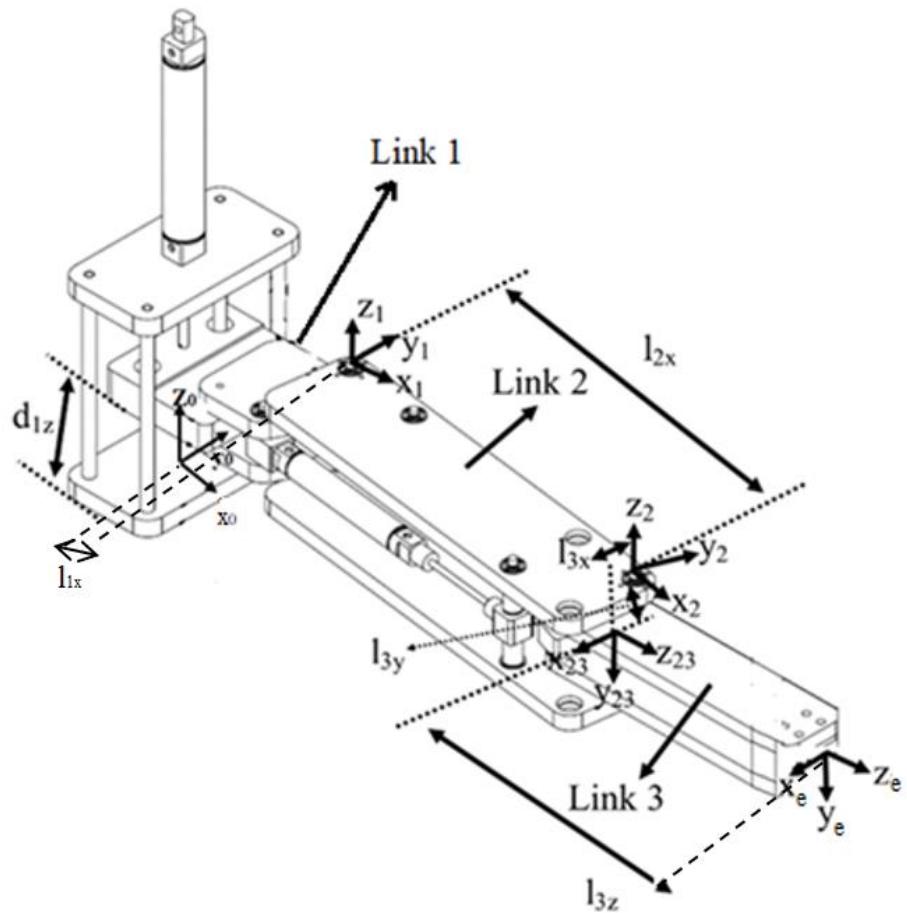
Figure 3-2. First device design (CAD model)

$$r^0_{end-effector} = T^0_e \, r^e_{end-effector} \tag{3.1}$$

$r^{\,0}_{end-effector}$ describes the end-effector position with respect to the global frame and

$r^3_{end-effector}$ describes the position of the end-effector with respect to the third frame. To derive the

transformation matrix (T^0_e) and using Figure 3-2, DH parameters can be excluded as follows as

shown in Table 1:

Table 1. DH parameters of first prototype

#	θ_i	d_i	a_i	α_i
0-1	0	d_{1z}	l_{1x}	0
1-2	θ_1	0	l_{2x}	0
2-23	$\theta_2 - 90$	l_{3y}	l_{3x}	-90
23-e	0	l_{3z}	0	0

$$T^n_{n+1} = \begin{bmatrix} c\theta_{n+1} & -s\theta_{n+1}\,c\alpha_{n+1} & s\theta_{n+1}\,s\alpha_{n+1} & a_{n+1}c\theta_{n+1} \\ s\theta_{n+1} & -c\theta_{n+1}c\alpha_{n+1} & -c\theta_{n+1}s\alpha_{n+1} & a_{n+1}s\theta_{n+1} \\ 0 & s\alpha_{n+1} & c\alpha_{n+1} & d_{n+1} \\ 0 & 0 & 0 & 1 \end{bmatrix} \tag{3.2}$$

To obtain the transformation matrix from the global frame to the end-effector frame, a successive set

of homogenous transformation matrices is used as follows:

$$T^0_e = T^0_1 \, T^1_2 \, T^2_{23} \, T^{23}_e \tag{3.3}$$

And:

$$T^0_1 = \begin{bmatrix} 1 & 0 & 0 & l_{1x} \\ 0 & 1 & 0 & 0 \\ 0 & 0 & 1 & d_{1z} \\ 0 & 0 & 0 & 1 \end{bmatrix} \tag{3.4}$$

$$T_2^1 = \begin{bmatrix} c\theta_1 & -s\theta_1 & 0 & l_{2x}c\theta_1 \\ s\theta_1 & c\theta_1 & 0 & l_{2x}s\theta_1 \\ 0 & 0 & 1 & 0 \\ 0 & 0 & 0 & 1 \end{bmatrix} \tag{3.5}$$

$$T_{23}^2 = \begin{bmatrix} s\theta_2 & 0 & c\theta_2 & l_{3x}s\theta_2 \\ -c\theta_2 & 0 & s\theta_2 & -l_{3x}c\theta_2 \\ 0 & -1 & 0 & l_{3y} \\ 0 & 0 & 0 & 1 \end{bmatrix} \tag{3.6}$$

$$T_e^{23} = \begin{bmatrix} 1 & 0 & 0 & 0 \\ 0 & 1 & 0 & 0 \\ 0 & 0 & 0 & l_{3z} \\ 0 & 0 & 0 & 1 \end{bmatrix} \tag{3.7}$$

By substituting equations (3.4), (3.5), (3.6) and (3.7) in (3.3)

$$T_e^0 = \begin{bmatrix} c\theta_1 s\theta_2 + s\theta_1 c\theta_2 & 0 & 0 & X \\ s\theta_1 s\theta_2 - c\theta_1 c\theta_2 & 0 & 0 & Y \\ 0 & -1 & 0 & Z \\ 0 & 0 & 0 & 1 \end{bmatrix} \tag{3.8}$$

X, Y, Z are the position of the end-effector with respect to the global frame $X_0 Y_0 Z_0$ and can be calculated as follows:

$$X = l_{3z}c\theta_1 c\theta_2 + l_{3x}c\theta_1 s\theta_2 - l_{3z} s\theta_1 s\theta_2 + l_{3x}s\theta_1 c\theta_2 + l_{2x} c\theta_1 + l_{1x} \tag{3.9}$$

$$Y = l_{3z}s\theta_1 c\theta_2 + l_{3x}s\theta_1 s\theta_2 + l_{3z} c\theta_1 s\theta_2 - l_{3x}c\theta_1 c\theta_2 + l_{2x} s\theta_1 \tag{3.10}$$

$$Z = l_{3y} + d_{1z} \tag{3.11}$$

The specifications of the first prototype are: l_{1x} =95 mm, l_{2x}=225.01 mm, l_{3x}=12.51 mm, l_{3y}=32.86 mm, l_{3z}=175 mm, d_{1z}=89 mm, $-60° \leq \theta_1 \leq 60°$ and $-60° \leq \theta_2 \leq 60°$, by substituting these values in equations (3.9), (3.10) and (3.11), the functions X, Y, Z can be obtained.

The workspace in $X_0 Y_0$ plane for the first prototype is shown in the following Figure 3-3
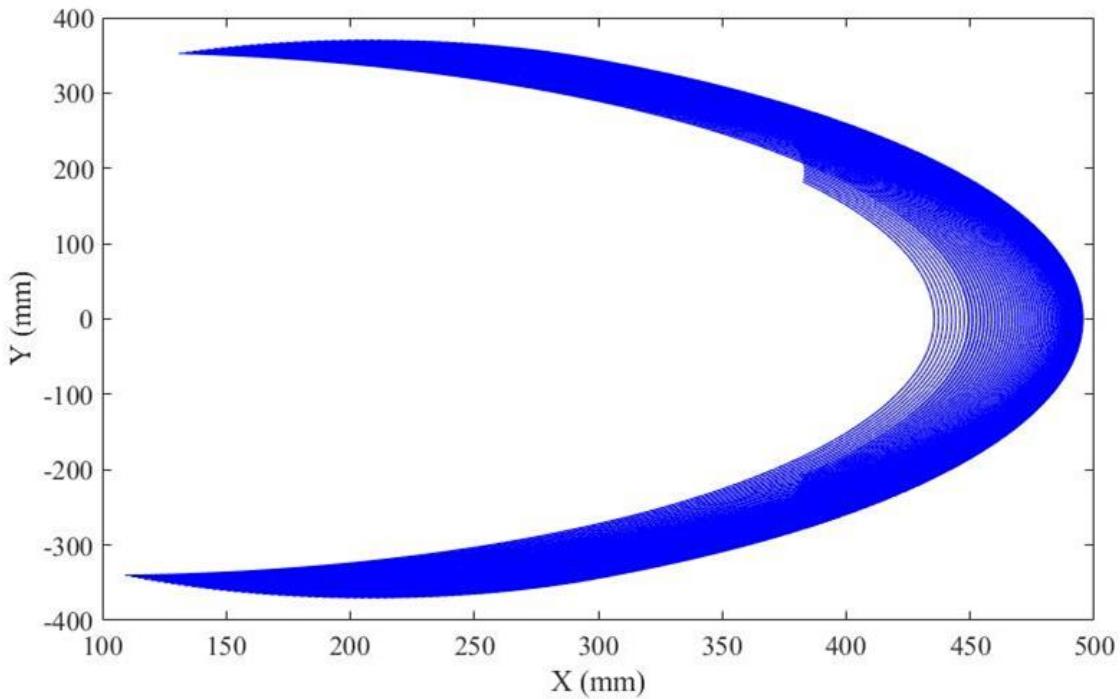
Figure 3-3. Workspace of first prototype in XY plane

Testing proved that this initial prototype was unsuccessful as a viable platform for wrist rehabilitation. The device failed to move without substantial friction along the *Z* axis. Additionally, its size made it too large to be used in fMRIs environments. From the lessons learned in the creation of this first prototype a second model was developed with the goal of reducing the overall size.

3.2.   Second prototype

The second iteration of the manipulandum (see Figure 3-4) sought to improve upon the design of

the previous version with a focus on overall weight and size reduction (see Figures 3-4 and 3-5)

[30].
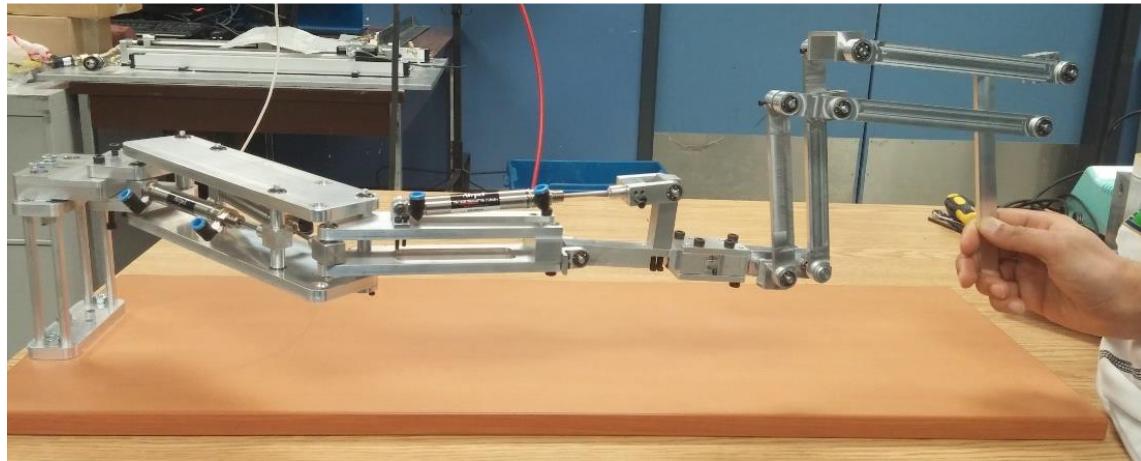
Figure 3-4. Second prototype device (source [30])
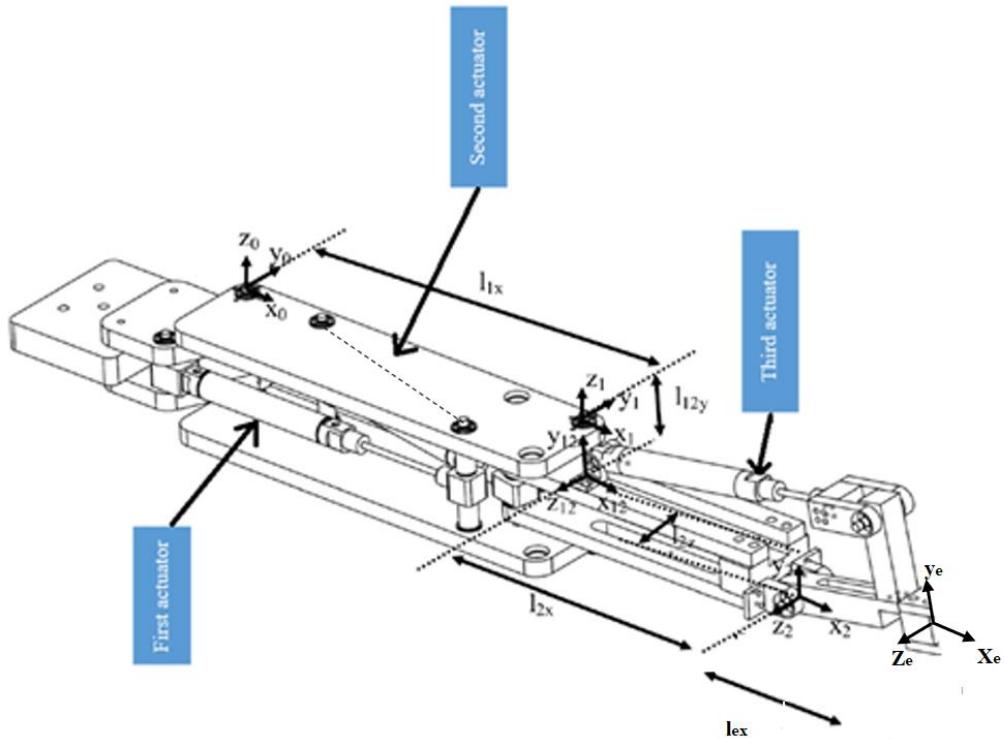
Figure 3-5. Second prototype, CAD model

As shown in Figure 3-5, all joints were revolute. The end-effector's position could be defined from the first three DOFs. The last two DOFs did not affect the position of the end-effector, their purpose was to change the end-effector's orientation, so they will not be considered when calculating the end-effector position with respect to the global frame.

To calculate the end-effector position with respect to the global frame $X_0 Y_0 Z_0$, the transformation matrix will be as follows:

$$r^0_{end-effector} = T^0_e \; r^e_{end-effector} \tag{3.12}$$

$r^0_{end-effector}$ is the position of the end-effector with respect to the global frame, $r^e_{end-effector}$ is the position of the end-effector with respect to the end-effector frame.

From Figure 3-5, DH parameters can be excluded as follows as shown in Table 2:

Table 2. DH parameters of second prototype

#	θ_i	d_i	a_i	α_i
0-1	θ_1	0	l_{1x}	0
1-12	θ_2	l_{12y}	0	$\frac{\pi}{2}$
12-2	0	l_{2z}	l_{2x}	0
2-e	θ_3	0	l_{ex}	0

The global transformation matrix is:

$$T^0_e = T^0_1 \; T^1_{12} \; T^{12}_2 T^2_e \tag{3.13}$$

By following the same procedure in calculating the transformation matrix for the first prototype. From Table 2:

18

$$T_1^0 = \begin{bmatrix} c\theta_1 & -s\theta_1 & 0 & l_{1x}c\theta_1 \\ s\theta_1 & c\theta_1 & 0 & l_{1x}s\theta_1 \\ 0 & 0 & 1 & 0 \\ 0 & 0 & 0 & 1 \end{bmatrix} \tag{3.14}$$

$$T_{12}^1 = \begin{bmatrix} c\theta_2 & 0 & s\theta_2 & 0 \\ s\theta_2 & 0 & -c\theta_2 & 0 \\ 0 & 1 & 0 & l_{12y} \\ 0 & 0 & 0 & 1 \end{bmatrix} \tag{3.15}$$

$$T_2^{12} = \begin{bmatrix} 1 & 0 & 0 & l_{2x} \\ 0 & 1 & 0 & 0 \\ 0 & 0 & 0 & l_{2z} \\ 0 & 0 & 0 & 1 \end{bmatrix} \tag{3.16}$$

$$T_e^2 = \begin{bmatrix} c\theta_3 & -s\theta_3 & 0 & l_{ex}c\theta_3 \\ s\theta_3 & c\theta_3 & 0 & l_{ex}s\theta_3 \\ 0 & 0 & 1 & 0 \\ 0 & 0 & 0 & 1 \end{bmatrix} \tag{3.17}$$

By substituting equations (3.14), (3.15), (3.16) and (3.17) in (3.13) T_e^0 will be as follows:

$$T_e^0$$

$$= \begin{bmatrix} c\theta_1c\theta_2c\theta_3 - s\theta_1s\theta_2c\theta_3 & -c\theta_1c\theta_2s\theta_3 + s\theta_1s\theta_2c\theta_3 & c\theta_1s\theta_2 + s\theta_1c\theta_2 & X \\ s\theta_1c\theta_2c\theta_3 + c\theta_1s\theta_2c\theta_3 & -s\theta_1c\theta_2s\theta_3 - c\theta_1s\theta_2s\theta_3 & s\theta_1s\theta_2 - c\theta_1c\theta_2 & Y \\ s\theta_3 & c\theta_3 & 0 & Z \\ 0 & 0 & 0 & 1 \end{bmatrix} \tag{3.18}$$

X, Y, Z are the end-effector position with respect to the global frame $X_0Y_0Z_0$, and can be calculated as follows:

$$X = l_{2z}c\theta_1s\theta_2 + l_{ex}c\theta_1c\theta_2c\theta_3 + l_{2x}c\theta_1c\theta_2 + l_{2z}s\theta_1c\theta_2 - l_{ex}s\theta_1s\theta_2c\theta_3$$
$$- l_{2x}s\theta_1s\theta_2 + l_{1x}c\theta_1 \tag{3.19}$$

$$Y = l_{2z}s\theta_1s\theta_2 + l_{ex}s\theta_1c\theta_2c\theta_3 + l_{2x}c\theta_1c\theta_2 - l_{2z}c\theta_1c\theta_2 + l_{ex}c\theta_1s\theta_2c\theta_3 \tag{3.20}$$
$$+ l_{2x}c\theta_1s\theta_2 + l_{1x}s\theta_1$$

$$Z = l_{1x}s\theta_3 + l_{12y} \tag{3.21}$$

The specifications of the second prototype are:

l_{1x} =164 mm, l_{2x}=135 mm, l_{ex}= 120 mm, l_{12y}=7mm, l_{2z}=15 mm, $0° \leq \theta_1 \leq 60°$, $-60° \leq \theta_2 \leq 0°$ and $-30° \leq \theta_3 \leq 30°$, by substituting these values in equations (3.19), (3.20) and (3.21), the functions X, Y, Z can be obtained. The workspace of the second prototype in $X_0 Y_0$ plane is shown in Figure 3-6.
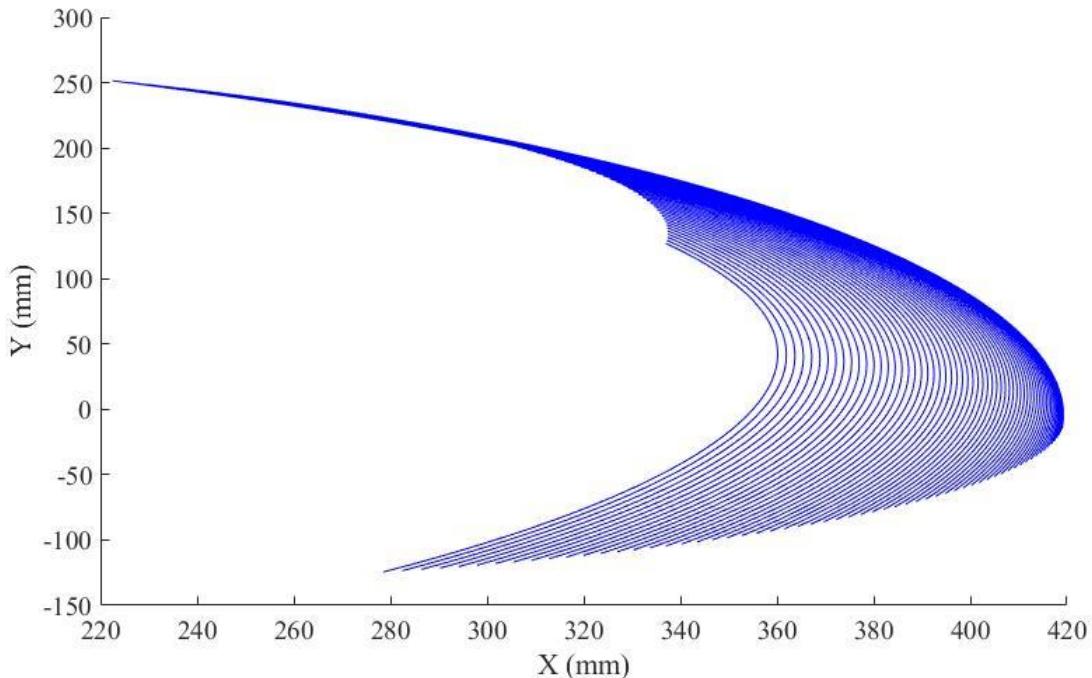
Figure 3-6. Workspace of second prototype in XY plane

The first and the second prototypes were made from aluminum and created using a CNC machine. They both used the *M16D100.0U* pneumatic actuators. The capability of mounting actuators inside the second prototype was better than the first one. The second prototype has also shown more effectiveness and smoothness. However, the size of both prototypes were still too big to use in fMRI applications.

3.3. Third prototype

In order to further reduce the overall size and weight of the device, the material used for the third prototype was changed from aluminum to acrylic. Acrylic was chosen due to its material properties which provide an adequate level of strength and rigidity while at a drastically lower weight than aluminum. There were many options for the actuator to reduce its size and stroke. For instance, *M9D12.5U* has a shorter stroke than the M16. That was the idea for the third prototype.

The third design was built using acrylic and the *M16D12.5U* pneumatic actuator. The advantage of using acrylic is that it is machinable. This allows for the use of manual milling and lathe machining to machine the prototype; however, the most accessible fabrication process for the acrylic applications was laser cutting. Compared with aluminum fabrication, laser-cutting fabrication is cheaper and faster. Figure 3-7 and Figure 3-8 show the third prototype.

All joints are revolute, the end-effector's position is defined from the first 3 DOFs. The last DOF is not actuated and does not affect the position of the end-effector, the purpose of the last DOF is to change the end-effector's orientation. So, it will be eliminated.
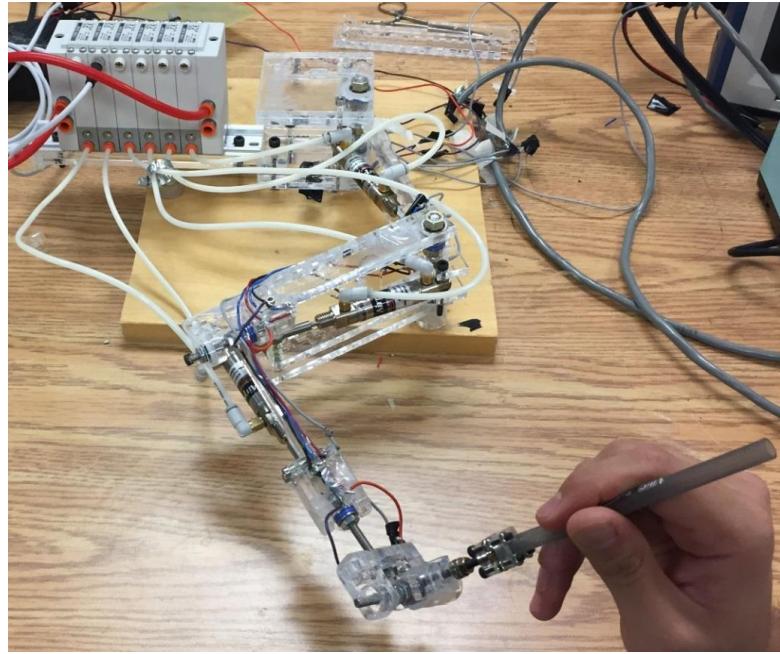
Figure 3-7. Third prototype device (source [30])
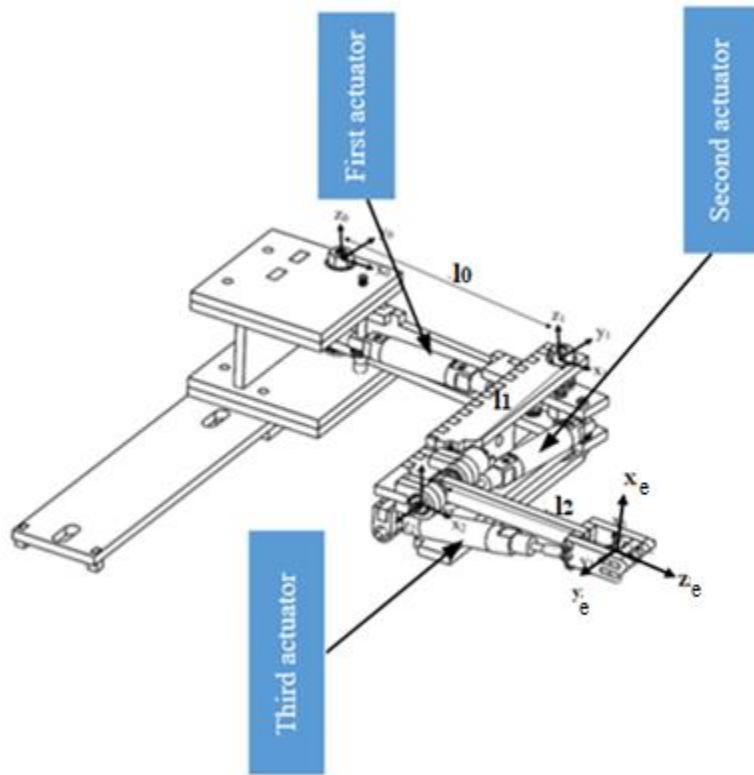
Figure 3-8. Free body diagram of third prototype

From the free body diagram (Figure 3-8) the DH parameters can be excluded and used to calculate the end-effector position with respect to the global frame [30].

To calculate the end-effector position with respect to the global frame, the transformation matrix will be as follows:

$$r^0_{end-effector} = T^0_3 \, r^3_{end-effector} \tag{3.22}$$

$r^0_{end-effector}$ is the position of the end-effector with respect to the global frame and $r^3_{end-effector}$ is the position of the end-effector with respect to the end-effector frame.

From Figure 3-8, DH parameter shown in Table 3 can be excluded as follows:

Table 3. DH parameters of third prototype

#	θ_i	d_i	a_i	α_i
0-1	θ_1	0	l_0	0
1-12	θ_2	0	0	$\frac{\pi}{2}$
12-2	0	l_1	0	0
2-23	$\theta_3 + \frac{\pi}{2}$	0	0	$\frac{\pi}{2}$
23-3	0	l_2	0	0

The global transformation matrix is:

$$T^0_e = T^0_1 \, T^1_{12} \, T^{12}_2 \, T^2_{23} \, T^{23}_e \tag{3.23}$$

By following the same procedure in calculating the transformation matrix for the first prototype.

From Table 3:

$$T_1^0 = \begin{bmatrix} c\theta_1 & -s\theta_1 & 0 & l_0 c\theta_1 \\ s\theta_1 & c\theta_1 & 0 & l_0 s\theta_1 \\ 0 & 0 & 1 & 0 \\ 0 & 0 & 0 & 1 \end{bmatrix} \qquad (3.24)$$

$$T_{12}^1 = \begin{bmatrix} c\theta_2 & 0 & s\theta_2 & 0 \\ s\theta_2 & 0 & -c\theta_2 & 0 \\ 0 & 1 & 0 & 0 \\ 0 & 0 & 0 & 1 \end{bmatrix} \qquad (3.25)$$

$$T_2^{12} = \begin{bmatrix} 1 & 0 & 0 & 0 \\ 0 & 1 & 0 & 0 \\ 0 & 0 & 1 & l_1 \\ 0 & 0 & 0 & 1 \end{bmatrix} \qquad (3.26)$$

$$T_{23}^2 = \begin{bmatrix} -s\theta_3 & 0 & c\theta_3 & 0 \\ c\theta_3 & 0 & s\theta_3 & 0 \\ 0 & 1 & 0 & 0 \\ 0 & 0 & 0 & 1 \end{bmatrix} \qquad (3.27)$$

$$T_e^{23} = \begin{bmatrix} 1 & 0 & 0 & 0 \\ 0 & 1 & 0 & 0 \\ 0 & 0 & 1 & l_2 \\ 0 & 0 & 0 & 1 \end{bmatrix} \qquad (3.28)$$

By substituting equations (3.24), (3.25), (3.26), (3.27) and (3.28) in (3.23), T_e^0 will be as follows:

T_e^0

$$= \begin{bmatrix} -c\theta_1 c\theta_2 s\theta_3 + s\theta_1 s\theta_2 s\theta_3 & c\theta_1 c\theta_2 + s\theta_1 c\theta_2 & c\theta_3(c\theta_1 c\theta_2 - s\theta_1 s\theta_2) & X \\ -c\theta_1 s\theta_2 s\theta_3 - s\theta_1 c\theta_2 s\theta_3 & s\theta_1 s\theta_2 - c\theta_1 c\theta_2 & c\theta_3(c\theta_1 s\theta_2 + s\theta_1 c\theta_2) & Y \\ c\theta_3 & 1 & s\theta_3 & Z \\ 0 & 0 & 0 & 1 \end{bmatrix} \quad (3.29)$$

X, Y, Z are the position of the end-effector with respect to the global frame $X_0 Y_0 Z_0$, and can be calculated as follows:

$$X = l_0 c\theta_1 + l_1(c\theta_1 s\theta_2 + s\theta_1 c\theta_2) + l_2(c\theta_1 c\theta_2 c\theta_3 - s\theta_1 s\theta_2 c\theta_3) \qquad (3.30)$$

$$Y = l_0 s\theta_1 - l_1(c\theta_1 c\theta_2 - s\theta_1 s\theta_2) + l_2(c\theta_1 s\theta_2 c\theta_3 - s\theta_1 c\theta_2 c\theta_3) \qquad (3.31)$$

$$Z = l_2 s\theta_3 \qquad (3.32)$$

The specifications of the second prototype are:

$l_0 = 150\ mm$, $l_1 = 165\ mm$, $l_2 = 108\ mm$, $l_3 = 50\ mm$, $-20° \leq \theta_1 \leq 20°$, $-40° \leq \theta_2 \leq 0°$ and $0° \leq \theta_3 \leq 40°$, by substituting these values in equations (3.30), (3.31), and (3.32), the functions X, Y, Z can be obtained. The workspace in $X_0 Y_0$ plane for the second prototype is shown in the following Figures 3-9.
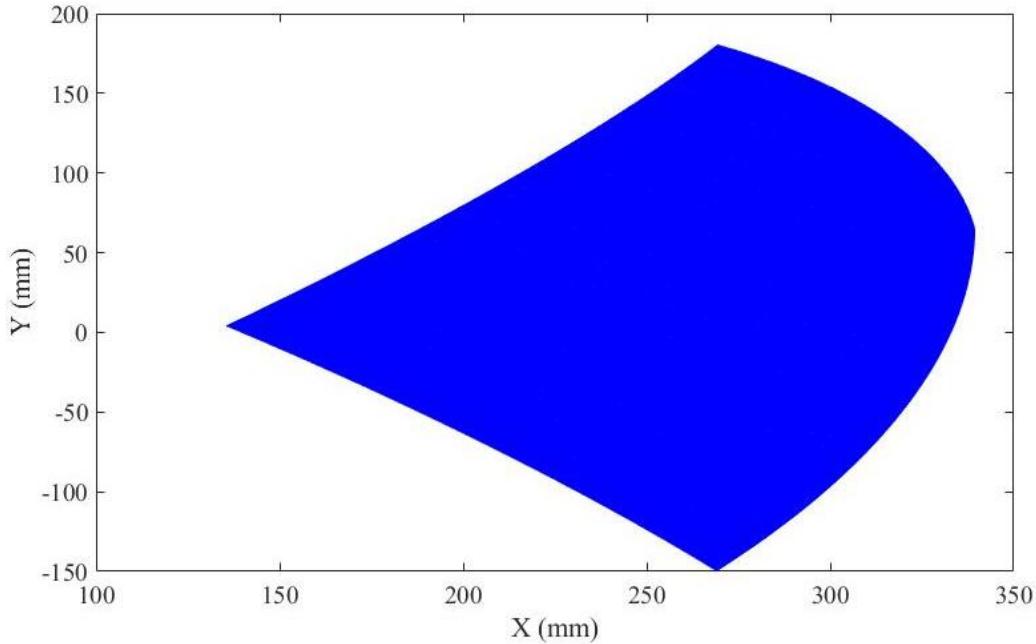
Figure 3-9. Workspace of third prototype in XY plane

The capability of mounting pneumatic actuators in the third prototype was better than the first and second prototypes. Rotary position sensors were used in the third prototype to define the position of each joint. The design lacked the rigidity to support itself and it failed due to the torsion. The design was not rigid enough to withstand the force of gravity. Moreover, the prototype did not fit for wrist motion rehabilitation.

A comparison between the final prototype and the previous three prototypes will be discussed in chapter 4.

4. Manipulandum Design

This chapter provides a detailed overview of the mechanical design for the final iteration of the manipulandum device developed in this thesis. This description highlights the wrist motions and design decisions that were chosen to specifically overcome the challenges of designing machines that move via pneumatic actuators – one of the challenges being the limitation in the actuator itself; for example, using 100 (mm) pneumatic actuator can only provide 15 (mm) linear movements. Attention was also placed on the structural complexities. This chapter describes a design that overcomes design challenges by providing an in-depth analysis of each of the arm-actuator parameters in a link-by-link fashion.

4.1. Wrist motions

The wrist is composed of complex joints around the carpal bones and the radius and forearm bones. The wrist is capable of three sets of various movements [31]:

- Flexion and extension

- Supination and pronation

- Ulnar deviation (ulnar flexion) and radial deviation (radial flexion)

Flexion describes the movement of bending the palm down, towards the wrist. Extension describes the movement of raising the back of the hand (see Figure 4-1 [31].
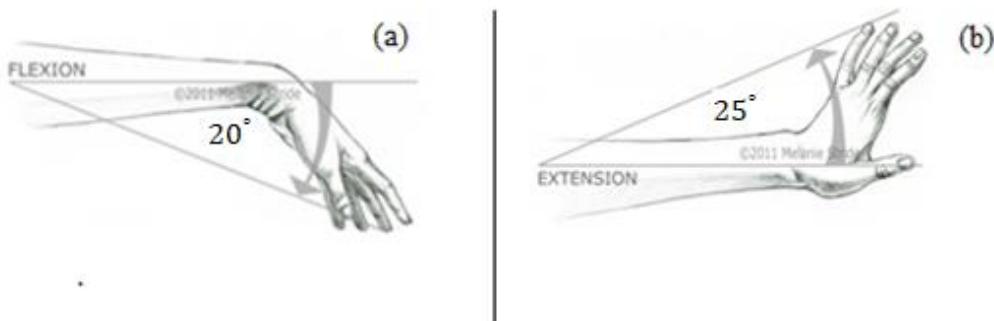
Figure 4-1. (a) Flexion and (b) extension movement of wrist (source [31])

26

Ulnar deviation, also known as ulnar flexion, is the movement of bending the wrist to the little finger, or ulnar bone, side. This is the movement you use when hitting the Enter key on a keyboard with the right hand. Radial deviation, also known as radial flexion, is the movement of bending the wrist to the thumb, or radial bone, side (see Figure 4-2) [32].
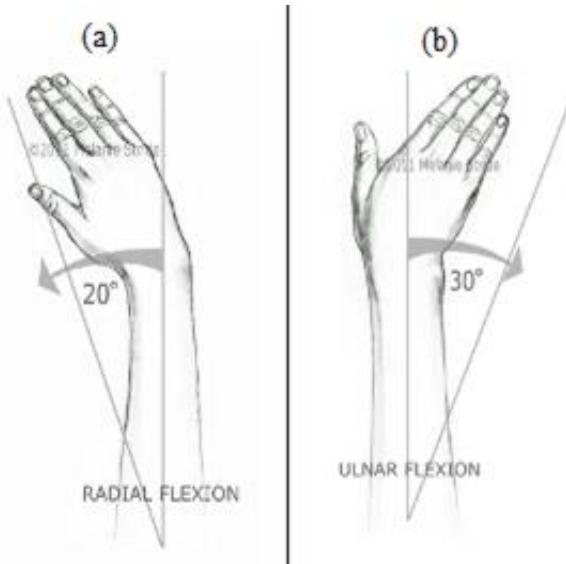
Figure 4-2. (a) Radial deviation and (b) ulnar deviation and motions of wrist (source [31])

Supination describes the movement of rotating the forearm into a palm up position. Pronation describes the movement of rotating the forearm into a palm down position. The supination and the pronation will not be tested in this thesis because the game requires the patient to move the paddle left and right in a liner motion while supination and pronation require a rotational motion (see Figure 4-3) [32].
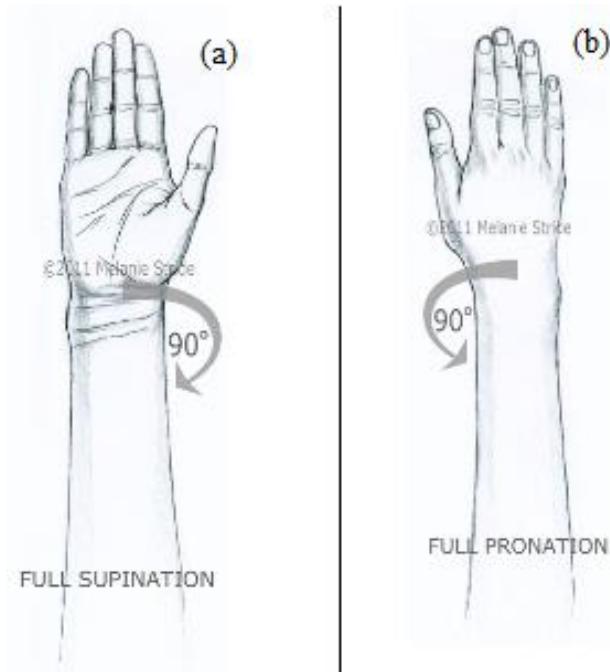
Figure 4-3. (a) Supination and (b) pronation motions of wrist (source [31])

The neutral position of the wrist is when the wrist is in straight alignment with the forearm, which is located at the mid-point between supination and pronation. This is commonly called the handshake position [31]. This position will be the neutral position (zero position) for the manipulandum that is designed in this thesis.

The targeted design is a handheld manipulandum that moves the wrist in flexion and extension. For the ulnar deviation and radial deviation, the wrist will be in the neutral position while holding the manipulandum. The adopted NFE game is a 2D game with an objective of catching the moving ball using a paddle that moves left and right.

4.2.   Design concept and workspace parameters

Multiple parameters need to be calculated in order to design the manipulandum, including the length of each link, the angle of the rotation of each joint, and the attached points of each actuator to the links. More importantly, the designed manipulandum must accommodate the required wrist motion in rehabilitation, which means that 2 DOF are needed: 1 DOF for the horizontal motion, and another DOF to allow the manipulandum to move up and down with the wrist. Since the actuator has only a 15 cm stroke length, which is not enough to keep up with wrist motion, another DOF will be needed to provide a larger workspace.

Figure 4-4 is a simplified design of a 3 DOF manipulandum.
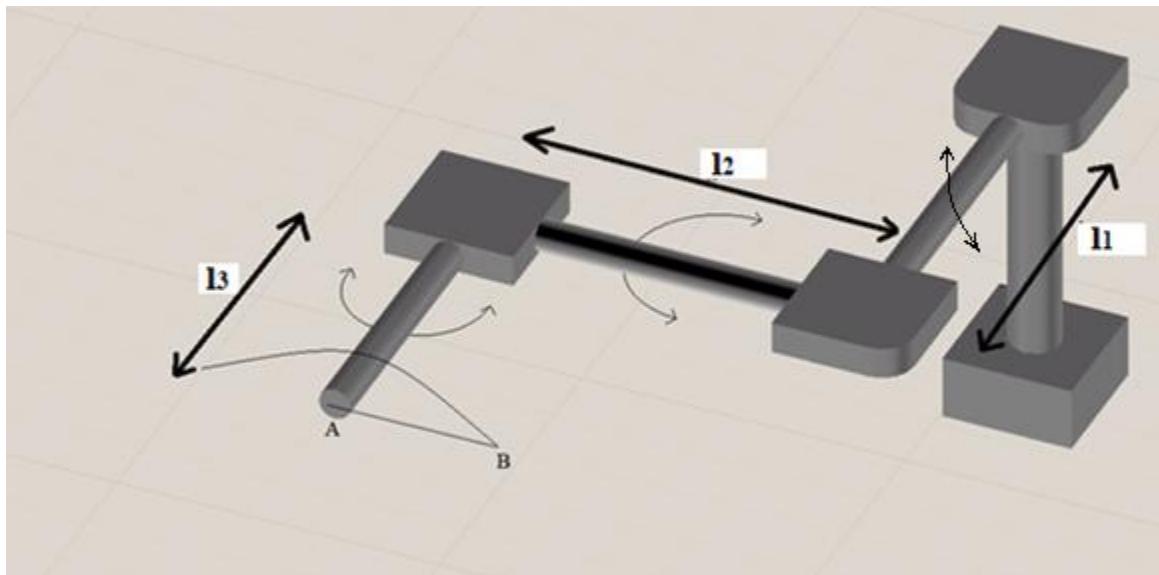
Figure 4-4. Simple 3 DOF manipulandum

The design requirements are established and compared for all of the arm-actuator configurations. The requirements are:

1. The workspace for each arm should be symmetric with respect to the horizontal plane.

2. The actuator force should be able to overcome the minimum required force while meeting the geometrical constraints.

The manipulandum consists of 3 actuated arms (see Figure 4-4). Each arm has two limitations: the mechanical actuator's extension and contraction limits. Both limitations must match the required generated angles for the symmetrical workspace.

The parameters for the workspace for each arm are shown in Figure 4-5. In order to make the motion symmetrical with respect to the horizon, l_1 and l_2 must be calculated.
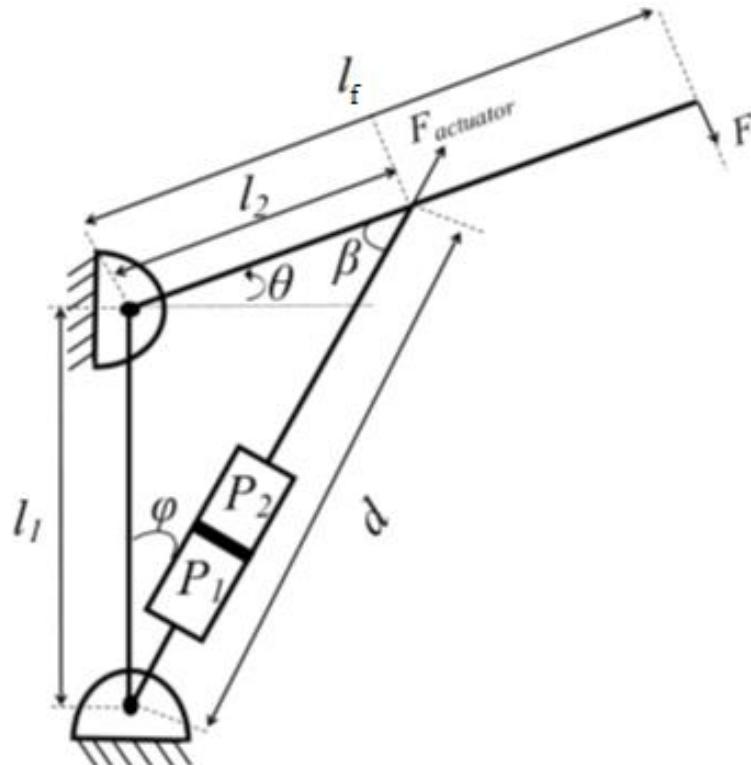
Figure 4-5. Arm-actuator workspace configuration

Since d in Figure 4-5 is changing based on the stroke length of the cylinder d_{min} represents the dimension d when the cylinder is fully retracted, and d_{max} represents the dimension d when the cylinder is fully extended. To calculate the workspace region, based on Figure 4-5, the parameters can be calculated as follows:

$$d^2 = l_1{}^2 + l_2{}^2 - 2l_1 \, l_2 cos(\frac{\pi}{2} + \theta) \tag{4.1}$$

$$d_{min}{}^2 = l_1{}^2 + l_2{}^2 - 2l_1 \, l_2 cos(\frac{\pi}{2} + \theta_{min}) \tag{4.2}$$

$$d_{max}{}^2 = l_1{}^2 + l_2{}^2 - 2l_1 \, l_2 cos(\frac{\pi}{2} + \theta_{max}) \tag{4.3}$$

A symmetrical workplace can only be achieved by satisfying the following equation:

$$\theta_{max} = -\theta_{min} \tag{4.4}$$

By substituting equation (4.4) in (4.2) and (4.3), the equation can be re-written as:

$$d_{min}{}^2 = l_1{}^2 + l_2{}^2 - 2l_1 \, l_2 \, sin(\theta_{max}) \tag{4.5}$$

$$d_{max}{}^2 = l_1{}^2 + l_2{}^2 + 2l_1 \, l_2 sin(\theta_{max}) \tag{4.6}$$

To calculate links l_1 and l_2 from equations (4.5) and (4.6) and after adjustments we get:

$$\frac{d_{min}^2 + d_{max}^2}{2} = l_1{}^2 + l_2{}^2 \tag{4.7}$$

$$\frac{d_{min}^2 - d_{max}^2}{4} = l_1 \, l_2 \, sin(\theta_{max}) \tag{4.8}$$

The final equation for l_1 and l_2 can be written as follows:

$$l_1 = \frac{\sqrt{\frac{d_{max}^2 + d_{min}^2}{2} + \frac{d_{max}^2 - d_{min}^2}{2sin(\theta_{max})}} + \sqrt{\frac{d_{max}^2 + d_{min}^2}{2} - \frac{d_{max}^2 - d_{min}^2}{2sin(\theta_{max})}}}{2} \qquad (4.9)$$

$$l_1 = \frac{\sqrt{\frac{d_{max}^2 + d_{min}^2}{2} + \frac{d_{max}^2 - d_{min}^2}{2sin(\theta_{max})}} - \sqrt{\frac{d_{max}^2 + d_{min}^2}{2} - \frac{d_{max}^2 - d_{min}^2}{2sin(\theta_{max})}}}{2} \qquad (4.10)$$

The first two parameters l_1 and l_2 have been defined by equations (4.9) and (4.10).

Any pneumatic actuator has limitation in its movements and its force. The limitation in movements is due to the available piston stroke length. The limitation in force is due to the amount of allowable pressure that the pneumatic actuator can tolerate at the rear or rod side.

$$\beta = \frac{\pi}{2} - (\varphi + \theta) \qquad (4.11)$$

and:

$$F\, l_f \cos(\theta) = F_{actuator}\, l_2 \sin(\beta) \qquad (4.12)$$

The equation (3.12) can be rewritten as:

$$F_{actuator} = \frac{F\, l_f \cos(\theta)}{l_2 \cos(\varphi + \theta)} \qquad (4.13)$$

The actuating force is force applied to the actuator in order to complete the intended operation. In this case, it is the force that is created by applying pressure to the rod end or the piston end of the pneumatic actuator. This can be written as:

$$F_{actuator} = P_1 A_1 - P_2 A_2 \qquad (4.14)$$

The angle (φ) can be determined from Figure 4-5 as follows:

$$l_2{}^2 = l_1{}^2 + \mathrm{d}^2 - 2l_1\, d\, cos(\varphi) \tag{4.15}$$

$$\varphi = cos^{-1}(\frac{(l_1{}^2 + \mathrm{d}^2) - l_2{}^2}{2\, d\, l_1}) \tag{4.16}$$

Various pneumatic actuators can be chosen that have the same parameters, but only some of them are fMRI-compatible. Therefore, the chosen actuator is M9D12.5U [30] which has 150 (mm) stroke length, a pressure ranges from 0.2 to 101.52 (psi), and a maximum force output of 139 (N) at the piston end side, which is enough to produce the required force and the required displacement, as will be discussed later in this chapter.

4.3. Design details

This section provides a detailed overview of analysing the parameters of each arm, the length of each joint, the rotation angle of each joint, and the attaching points of actuators.

4.3.1. First actuating arm

The specification for the first actuating arm is:

$F = 10$ (N), $l_f = 157$ (mm), $l_1 = 113.41$ (mm), $l_2 = 20$ (mm), and $\theta_{max} = 23$ (deg), $\theta_{min} = -23$ (deg), $d_{min} = 105$ (mm), $d_{max} = 120$ (mm), by substituting these values in (4.16) and (4.13), each of φ and $F_{actuator}$ can be calculated.

Figure 4-6 shows the relationship between the first joint angle and the actuating force. The value of φ is decreasing from 12 (deg) and 8.2 (deg) which satisfies the fact from Figure 4-5, where φ is decreasing while θ is increasing. F actuator in Figure 4-6 represents the minimum required force that the chosen actuator must generate, F=10 represents the wrist force and θ is the joint angle.
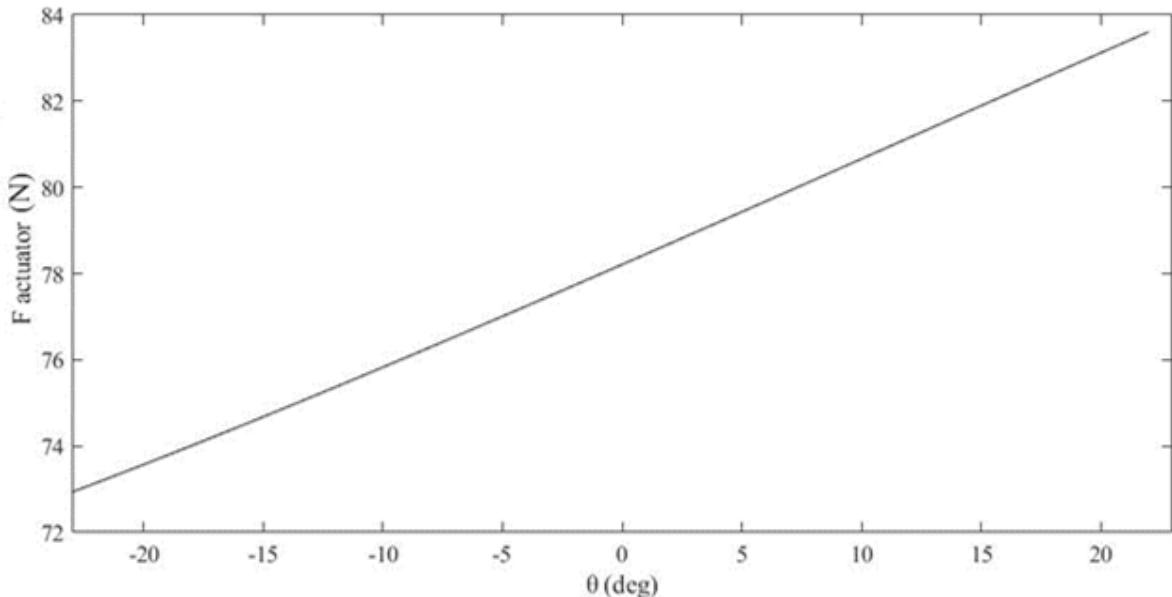

Figure 4-6. Actuating force versus joint angle (first arm)

34

4.3.2. Second actuating arm

The second arm parameters are nearly identical to the first arm but with a slight difference. The first arm plane is XZ, while the second arm plane is -XY. The specification for the second actuating arm is:

$F = 10$ (N), $l_f = 145$ (mm), $l_1 = 105$ (mm), $l_2 = 25$ (mm), and $\theta_{max} = 23$ (deg), $\theta_{min} = -23$ (deg). $d_{min} = 105(mm)$, $d_{max} = 120$ (mm), by substituting these values in (4.16) and (4.13), each of φ and $F_{actuator}$ can be calculated. Figure 4-7 shows the relationship between $F_{actuator}$ and the second joint angle θ where value of φ is changing from 77.5 (deg) and 25.5 (deg).
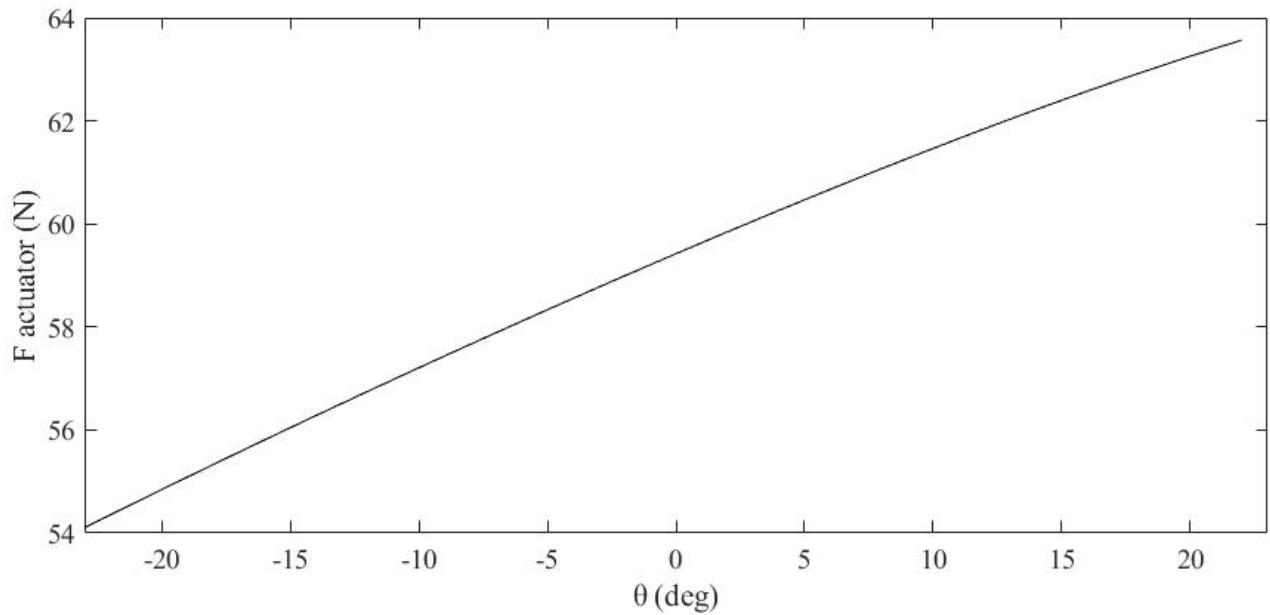

Figure 4-7. Actuating force versus joint angle (second arm)

4.3.3. Third actuating arm

The third arm parameters are the same as the first and second arm parameters. The only difference is that the first arm plane is XZ, the second arm plane is -XY, while the third arm plane is X-Y. The specification for the third actuating arm is:

$F = 10$ (N), $l_f = 155$ (mm), $l_1 = 105$ (mm), $l_2 = 22$ (mm), and $\theta_{max} = 23$ (deg), $\theta_{min} = -23$ (deg).

$d_{min} = 105$ (mm), $d_{max} = 120$ (mm), by substituting these values in (3.16) and (3.13), each of φ and $F_{actuator}$ can be calculated. Figure 4-8 shows the relationship between $F_{actuator}$ and θ the joint angle for the third actuating arm.
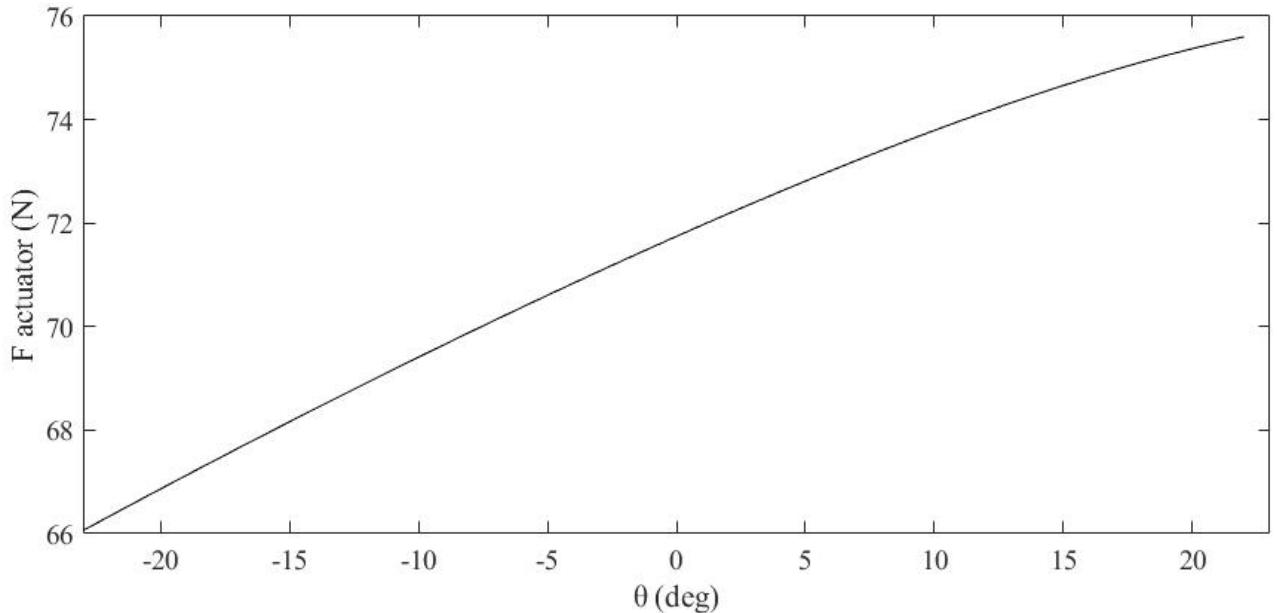

Figure 4-8. Actuating force versus joint angle (third arm)

The actuator force $F_{actuator}$ (shown in Figures 4-6, 4-7 and 4-8) does not exceed the maximum force limit of the chosen actuator, which is 139 (N). This means that the actuator is able to compensate for the required force.

Figure 4-9 shows the relationship between the actuating force $F_{actuator}$ and the third joint motion where d changes from 105 (mm) to 120 (mm).
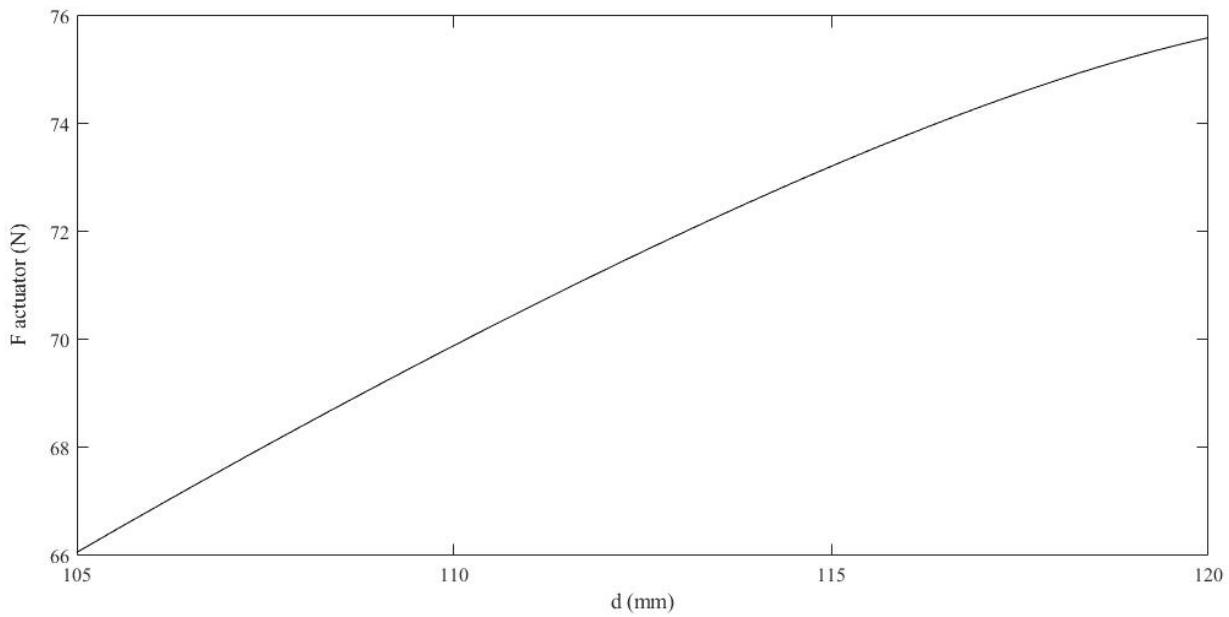

Figure 4-9. Actuating force versus third joint motion

4.4.   Final design

The idea for the final prototype was to design a manipulandum which is; smaller than the previous designs, made from a lighter material, uses the M9D12.5U pneumatic actuator to get the minimal stroke size and is fit for wrist motion rehabilitation - which means the prototype should be fMRI-compatible. The final design was built using thermoplastic which is commercially available and can be fabricated to any model by using a 3D printer, which is the most affordable fabrication process for the thermoplastic. Compared with aluminum fabrication and laser cutting fabrication, 3D printing is cheaper, faster and more durable. Moreover, 3D printing fabrication can be designed to hold more torsion.
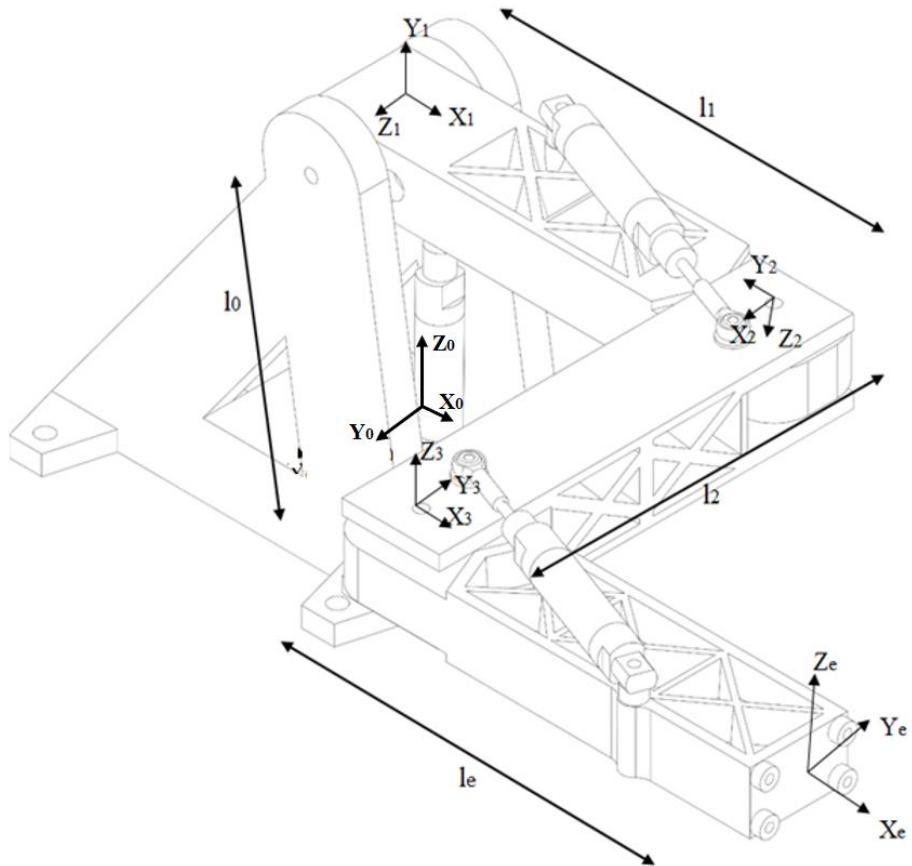

Figure 4-10. Final prototype

As shown in Figure 4-9, the final prototype has 3 DOF. All joints are revolute and the end-effector's position can be defined from the 3 DOFs. Those 3 DOF control the end-effector's orientation and position.

To calculate the end-effector's position with respect to the global frame, the transformation matrix will be as follows:

$$r^0_{end-effector} = T^0_e \, r^e_{end-effector} \tag{4.17}$$

where: $r^0_{end-effector}$ is the position of the end-effector with respect to the global frame and $r^e_{end-effector}$ is the position of the end-effector with respect to the end-effector frame.

From Figure 4-9, DH parameters can be excluded as follows in Table 4:

Table 4. DH parameters of final prototype

Link number	θ_i	d_i	a_i	α_i
0-1	0	l_0	0	0
1-2	$\theta_1 + 90$	0	l_1	90
2-3	$90 - \theta_2$	0	l_2	180
3-e	θ_3	0	l_e	0

The global transformation matrix is:

$$T^n_{n+1} = \begin{bmatrix} c\theta_{n+1} & -s\theta_{n+1}\,c\alpha_{n+1} & s\theta_{n+1}\,s\alpha_{n+1} & a_{n+1}c\theta_{n+1} \\ s\theta_{n+1} & -c\theta_{n+1}c\alpha_{n+1} & -c\theta_{n+1}s\alpha_{n+1} & a_{n+1}s\theta_{n+1} \\ 0 & s\alpha_{n+1} & c\alpha_{n+1} & d_{n+1} \\ 0 & 0 & 0 & 1 \end{bmatrix} \tag{4.18}$$

The global transformation matrix is:

$$T^1_4 = T^1_2 \, T^2_3 \, T^3_4 \tag{4.19}$$

and:

$$T_1^0 = \begin{bmatrix} 1 & 0 & 0 & 0 \\ 0 & -1 & 0 & 0 \\ 0 & 0 & 1 & l_0 \\ 0 & 0 & 0 & 1 \end{bmatrix} \tag{4.20}$$

$$T_2^1 = \begin{bmatrix} -s\theta_1 & 0 & c\theta_1 & -l_1 s\theta_1 \\ c\theta_1 & 0 & s\theta_1 & l_1 c\theta_1 \\ 0 & 1 & 0 & 0 \\ 0 & 0 & 0 & 1 \end{bmatrix} \tag{4.20}$$

$$T_3^2 = \begin{bmatrix} s\theta_2 & -c\theta_2 & 0 & l_2 s\theta_2 \\ c\theta_2 & -s\theta_2 & 0 & l_2 c\theta_2 \\ 0 & 0 & 1 & 0 \\ 0 & 0 & 0 & 1 \end{bmatrix} \tag{4.21}$$

$$T_e^3 = \begin{bmatrix} c\theta_3 & -s\theta_3 & 0 & l_3 c\theta_3 \\ s\theta_3 & -c\theta_3 & 0 & l_3 s\theta_3 \\ 0 & 0 & 1 & 0 \\ 0 & 0 & 0 & 1 \end{bmatrix} \tag{4.22}$$

By substituting equations (4.20, 4.21, and 4.22) in (4.19) we get the global transformation matrix as follows:

$$T_{end-effector}^0$$

$$= \begin{bmatrix} s\theta_1 c\theta_2 s\theta_3 - s\theta_1 s\theta_2 c\theta_3 & s\theta_1 s\theta_2 s\theta_3 - s\theta_1 c\theta_2 c\theta_3 & c\theta_1 & X \\ c\theta_1 c\theta_2 s\theta_3 - c\theta_1 s\theta_2 c\theta_3 & c\theta_1 s\theta_2 s\theta_3 - c\theta_1 c\theta_2 c\theta_3 & -s\theta_1 & Y \\ c\theta_2 c\theta_3 - s\theta_2 s\theta_3 & s\theta_2 c\theta_3 - c\theta_2 s\theta_3 & 0 & Z \\ 0 & 0 & 0 & 1 \end{bmatrix} \tag{4.23}$$

Where X, Y, Z are the position of the end-effector with respect to the global frame $X_0 Y_0 Z_0$ and can be calculated as follows:

$$X = -l_1 s\theta_1 - l_2 s\theta_1 s\theta_2 + l_3(s\theta_1 c\theta_2 s\theta_3 - s\theta_1 s\theta_2 c\theta_3) \tag{4.24}$$

$$Y = -l_1 c\theta_1 - l_2 c\theta_1 s\theta_2 + l_3(c\theta_1 c\theta_2 c\theta_3 - c\theta_1 s\theta_2 c\theta_3) \tag{4.25}$$

$$Z = l_0 + l_2 c\theta_2 + l_3(c\theta_2 c\theta_3 - s\theta_2 s\theta_3) \tag{4.26}$$

The specification of the first prototype are:

l_1 =151 mm, l_2=143 mm, l_3=154 mm, $-23° \leq \theta_1 \leq 23°$, $-23° \leq \theta_2 \leq 23°$ and $-23° \leq \theta_3 \leq 23°$, by substituting these values in equations (4.24, 4.25 and 4.26), the functions X, Y, Z can be obtained. The workspace in the $X_0 Y_0$ plane for the final prototype is shown in the following Figures 4-10.
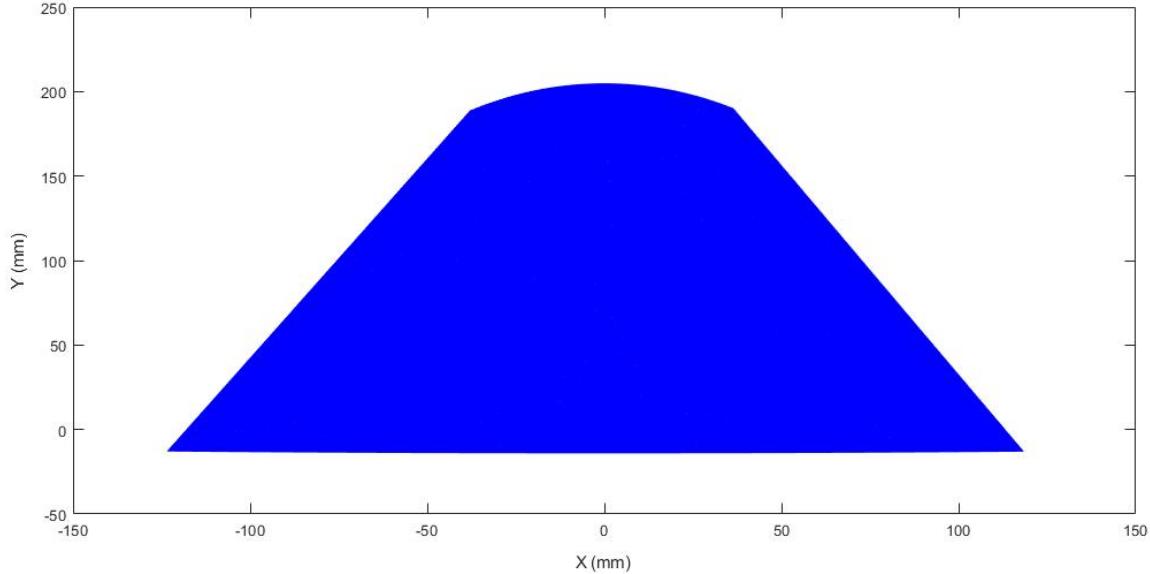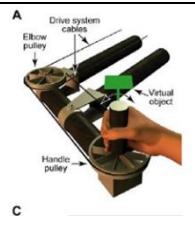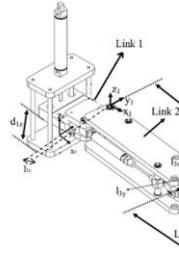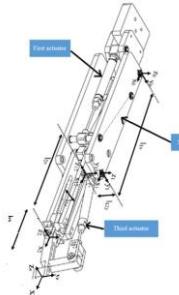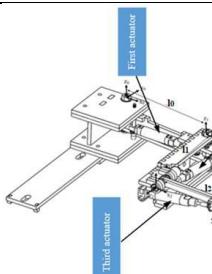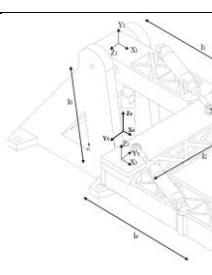


Figure 4-11. 2D workspace of final prototype XY plane

Compared to aluminum (the first and the second prototype) and acrylic (the third prototype), thermoplastic is commercially cheaper and easier to model. This is because, firstly, only a 3D printer is needed to print the design. Secondly, using thermoplastic made the final design lighter than the previous prototypes. Moreover, the rigidity to withstand the gravity force and the size of the final design made this concept superior to the previously developed prototypes. Additionally, the workspace of the final prototype in the XY plane (see Figure 4-11) is comparatively larger than the workspace of the previous three prototypes (see Figures 3-3, 3-6 and 3-9). It allows for a greater range of motion for the patient at 120 (mm) of wrist rotation in each direction. Finally, the symmetrical nature of the workspace in the final prototype made playing the NFE game more accessible to the patients.

Table 5 compare between the three previous prototypes and the final prototype. Rectangle size is the maximum rectangle size that can fit inside workspace

Table 5. Previous prototypes comparison

Prototype name	Material	Machining	Actuators type	Rectangle size	fMRI compatibility	Wrist rehab applicability	CAD model
WristBOT manipulan dum	Magnetic material	-	Electrical	-	No	Yes	
phantom omni haptic device	Magnetic material	-	Electrical	-	No	No	
1st prototype	Aluminum	CNC machining	Pneumatic	16x101 mm^2	No	No	
2nd prototype	Aluminum	CNC machining	Pneumatic	50x300 mm^2	No	No	

3rd prototype	Acrylic	Laster cutting machining	Pneumatic	87x161 mm^2	Yes	No	
Final prototype	Thermoplastic	3D printing	Pneumatic	150x125 mm^2	Yes	Yes	

Euler angles

A rotation of ψ radians about the x-axis is defined as $R_x(\psi)$, a rotation of θ radians about the y-axis is defined as $R_y(\theta)$ and a rotation of φ radians about the z-axis is defined as $R_z(\varphi)$, where the angles ψ, θ, and φ are the Euler angles.

$$R_x(\psi) = \begin{bmatrix} 1 & 0 & 0 \\ 0 & c\psi & -s\psi \\ 0 & s\psi & c\psi \end{bmatrix} \tag{4.27}$$

$$R_y(\theta) = \begin{bmatrix} c\theta & 0 & s\theta \\ 0 & 1 & 0 \\ -s\theta & 0 & c\theta \end{bmatrix} \tag{4.28}$$

$$R_z(\varphi) = \begin{bmatrix} c\varphi & -s\varphi & 0 \\ s\varphi & c\varphi & 0 \\ 0 & 0 & 1 \end{bmatrix} \tag{4.29}$$

The general rotation matrix has the form:

$$R = R_z(\varphi)\, R_y(\theta)\, R_x(\psi) = \begin{bmatrix} R_{11} & R_{12} & R_{13} \\ R_{21} & R_{22} & R_{23} \\ R_{31} & R_{32} & R_{33} \end{bmatrix} \tag{4.30}$$

Equation (4.30) result to:

$$R = \begin{bmatrix} c\theta c\varphi & s\psi s\theta c\varphi - c\psi s\varphi & c\psi s\theta c\varphi + s\psi s\varphi \\ c\theta s\varphi & s\psi s\theta s\varphi + c\psi c\varphi & c\psi s\theta s\varphi - s\psi c\varphi \\ -s\theta & s\psi s\theta & c\psi s\theta \end{bmatrix} \tag{4.31}$$

We can compute the Euler angles ψ, θ, and φ by equating each element in R with the corresponding element in the matrix product $R_z(\varphi)\, R_y(\theta)\, R_x(\psi)$.

$$R_{31} = -s\theta \tag{4.32}$$

This equation can be inverted into:

$$\theta = -s^{-1}(R_{31}) \tag{4.33}$$

To find the value of ψ, we observe that:

$$\frac{R_{32}}{R_{33}} = \tan{(\psi)} \tag{4.35}$$

This equation can be inverted into:

$$\psi = \text{atan2}(R_{32}, R_{33}) \tag{4.36}$$

A similar analysis holds for finding φ, which can be observed as follows:

$$\frac{R_{21}}{R_{11}} = \tan{(\varphi)} \tag{4.37}$$

This equation can be inverted into:

$$\varphi = \text{atan2}(R_{21}, R_{11}) \tag{4.38}$$

The general transformation matrix (4.23) can be written as follows:

$$T^0_{end-effector} = \begin{bmatrix} R_{11} & R_{12} & R_{13} & X \\ R_{21} & R_{22} & R_{23} & Y \\ R_{31} & R_{32} & R_{33} & Z \\ 0 & 0 & 0 & 1 \end{bmatrix} \tag{4.39}$$

By substituting the values of R_{31}, R_{32}, R_{33}, R_{21} and R_{11} in the equations (4.33), (4.36) and (4.38), Euler angles can be re-written as follows:

$$\theta = -sin^{-1}(c\theta_2 c\theta_3 - s\theta_2 s\theta_3) \tag{4.40}$$

$$\psi = \text{atan2}(s\theta_2 c\theta_3 - c\theta_2 s\theta_3, 0) \tag{4.41}$$

$$\varphi = \text{atan2}(c\theta_1 c\theta_2 s\theta_3 - c\theta_1 s\theta_2 c\theta_3 , s\theta_1 c\theta_2 s\theta_3 - s\theta_1 s\theta_2 c\theta_3) \tag{4.42}$$

Where θ, ψ, φ represent the orientation of the end-effector with respect to the global frame $X_0 Y_0 Z_0$.

The sensor that is used in the final prototype is a wireless mouse (will be discussed in chapter 5 and chapter 6). The wireless mouse has a built-in gyroscope. In another wards, if the sensor is attached to the end-effector θ, ψ, φ represent the orientation of the sensor and X, Y, Z represent the location of it. These values (θ, ψ, φ, X, Y, Z) is used to move the end-effector diagonally.

5. Prototype Device

This chapter describes all of the considerations that went into the fabrication of the final version manipulandum, including the manufacturing methods and the selection of hardware components. In addition to the physical links described in Chapter 4 many additional components are required for the device to properly actuate including a reservoir, pressurized air, valves, a pressure regulator and a control circuit, which are all generally employed to develop a pneumatic manipulandum. The reservoir provides the air pressure and the valves then control the direction of the pressurized air. The control circuit sends a command signal to control the valves.

5.1. Hardware components

Many components come together to form the final design for the final prototype (see Figure 5-1). The prototype has 3 links; each link represents 1 DOF and is actuated by a pneumatic double acting cylinder M9D12.5U [32]. These pneumatic actuators receive the pressurized air from the valves SMC ITV0030 [33] shown in Figure 5-3. Two valves are needed to control each cylinder. The valves receive the signal from the Quanser control board Q8 shown in Figure 5-4. The pressure regulator SMC ITV1050 [34] shown in Figure 5-5 receives the command signal from the control circuit and provides pressure to the actuators based on the value of the command signal. The feedback of the system is the position of the wireless mouse (shown in Figure 5-6) that is attached to the third link.

Figure 5-7 shows the full set up including the 3 DOF pneumatic acutated maipulandom, the wireless mouse, the directional control valves (DCVs), the board and the connected PC.
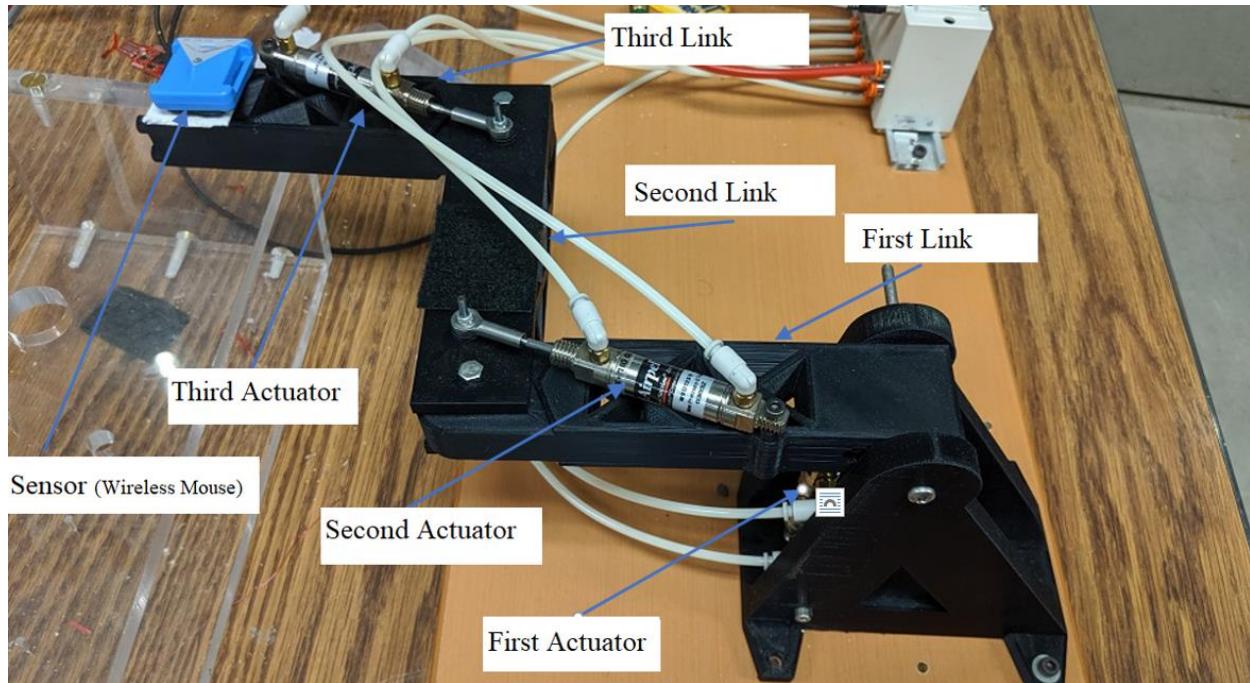
Figure 5-1. 3 DOF final manipulandum
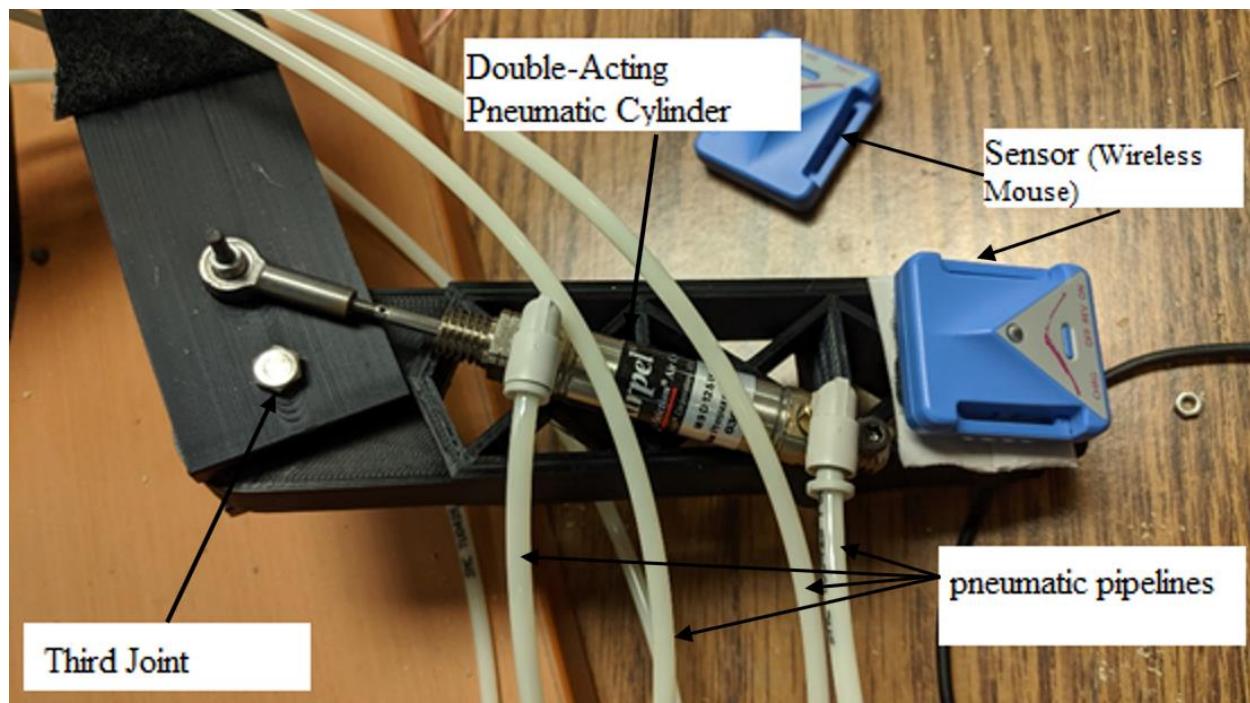
Figure 5-2. Location of wireless mouse

Figure 5-3. Pressure control valves are SMC ITV0030 [33]

Figure 5-4. Q8 Quanser board

Figure 5-5. Pressure regulator SMC ITV1050 [34]

Figure 5-6. Mobility research wireless mouse
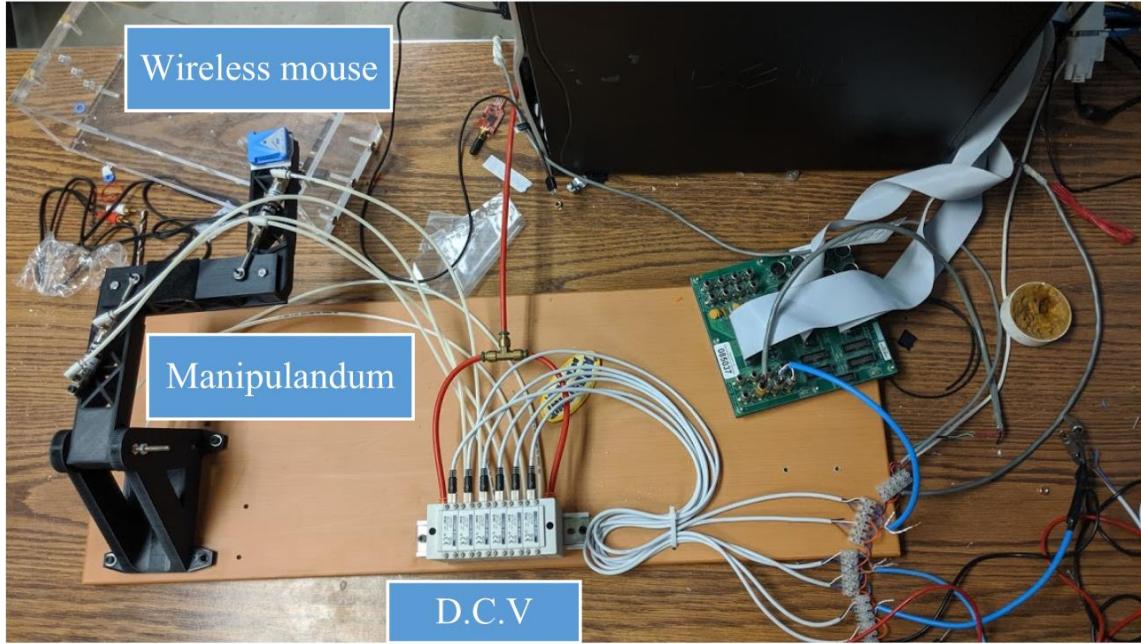
Figure 5-7. Full set up of final manipulandum

The wired sensor had overshooting in its signal that created problems for the controlling process. One of these problems was that the overshoot required many low-pass filters which increased the processing and response time. To improve upon this, the final design makes use of an easy to install wireless mouse (shown in Figure 5-6) attached to the manipulandum as shown in Figure 5-1 and Figure 5-2. The wireless mouse has a high accuracy and is available for research purposes in the Rehabilitation Centre in Winnipeg. Only the position of the mouse is needed which can be obtained using a function that exists in the MATLAB.

5.2. Software

The software that is used to get the input data is an NFE game (Neuro Function Evaluation). In this thesis it is a 2D game as shown in Figure 5-8. The game is currently being used in the Rehabilitation Centre in Winnipeg, Manitoba for research and rehabilitation purposes. As the patient plays the game their movements are tracked in real-time and their performance is exported as data that can be assessed by health care professionals. This quantitative data is able to provide tangible data based on accuracy. Furthermore, many modes, such as assistive, resistive and assistive when required, can be used based on the individual patient's recovery process.
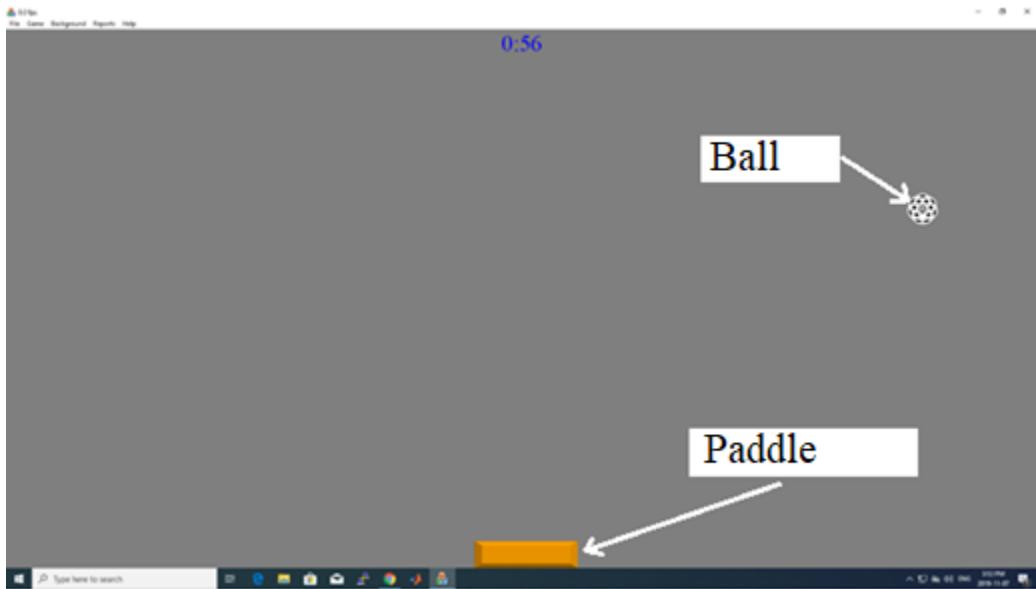

Figure 5-8. Neuro Function Evaluation GAME Digital Rehab

The feedback of the wireless mouse is the position of the paddle; the reference is zero at the beginning of the experiment; the measured error is the difference between the location of the ball and the location of the paddle; the interface of the controller is a MATLAB Simulink; and the output is a voltage signal that ranges between 0-10 Volts and goes to the pressure regulator which applies pressure (0 to 100 psi). The pressurized air goes to the pneumatic actuator to apply motion. This will be discussed further in the next chapter.
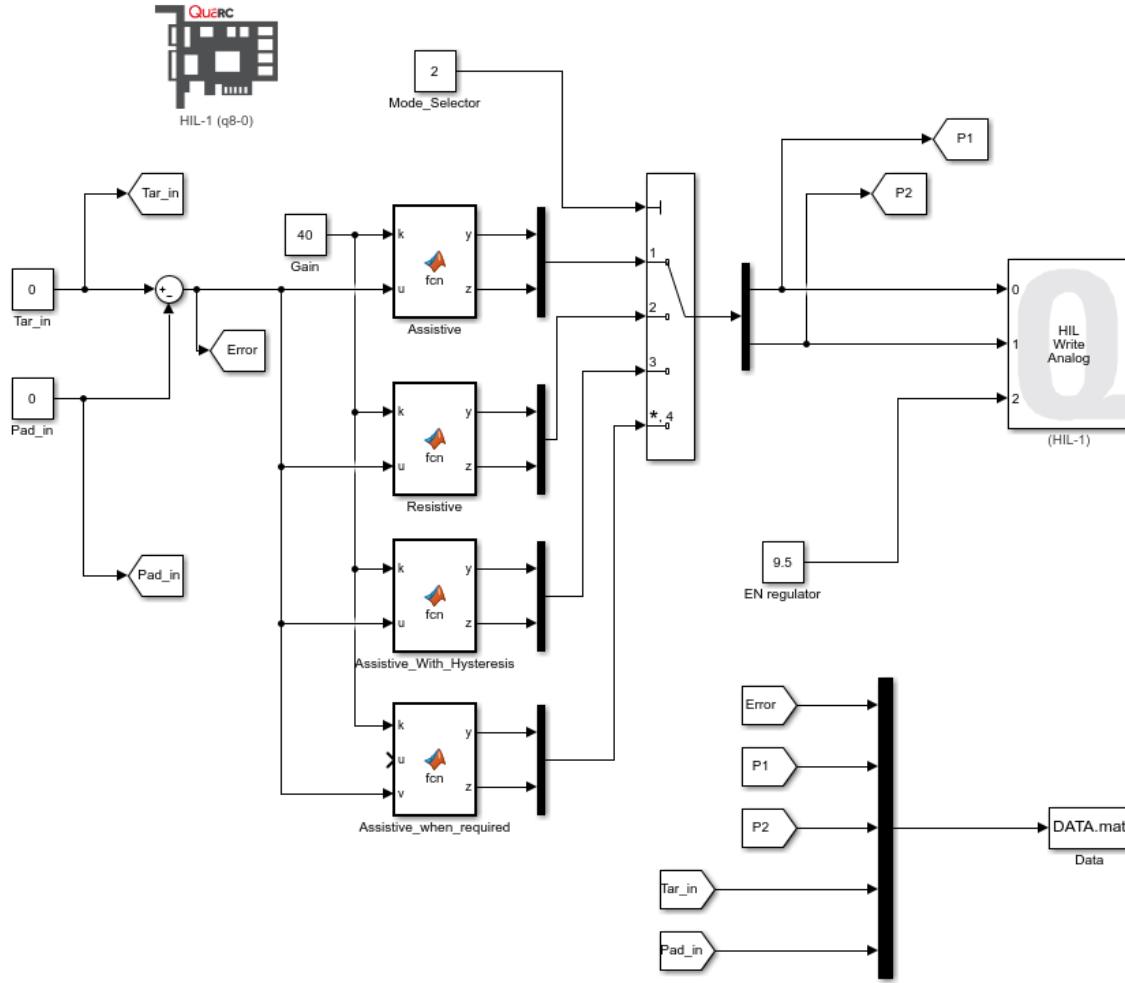
Figure 5-9. MATLAB Simulink manipulandum interface

Block Tar_in receives the data from the MATLAB workspace which has the value of the location of the ball. Block Pad_in does the same for the location of the paddle. Block mode selector is to switch between modes (assistive, resistive, assistive with hysteresis, assistive when required). Block P1 saves the value of the extent pressure and block P2 saves the value of the retract pressure. Block HIL-1(q8-0) is the Quanser board and block (HIL-1) writes the values of P1 and P2 on the Quanser board. Block Data saves the values of the errors P1, P2, Tar_in and Pad_in in an excel file. All these values will be used in the next chapter to evaluate the performance of the final prototype.

52

6. Performance Evaluation

This chapter starts by presenting the analysis of the third joint (since the NFE GAME is a 2D game so only one joint will be needed to run the game), then moves to validating data between the wrist and the robot to match the data between the wrist and the manipulandum, and finishes with the performance analysis of the manipulandum in three modes (assistive, resistive, and assistive with hysteresis). In the assistive mode the manipulandum will assist the patient to move the paddle (see Figure 5-8) towards catching the falling ball. In the resistive mode the manipulandum acts as a resistive force against the patient, applying pressure as the patient gets closer towards the ball, with the goal of preventing the patient from moving the paddle towards the ball. The assistive mode with hysteresis is similar to assistive mode with the difference being that the manipulandum will assist the patient to move the paddle towards the ball for a certain distance. These three modes will be discussed later in this chapter.

6.1. Wrist and manipulandum motion relation

The purpose of this section is to prove that the third joint represents the motion of the wrist when the wrist is moving horizontally in the XY plane (as shown in Figure 6-1). In order to do that the motion of the third and the second joints will be analysed.

The average radius of the rotation that leads to liner displacement of the wrist is 10 (cm). The wrist is holding the endpoint of the end-effector. When the wrist is rotating, the manipulandum will be moving from point A to point B on an arc (shown in Figure 6-1). The arc represents the horizontal rotational motion of the wrist.
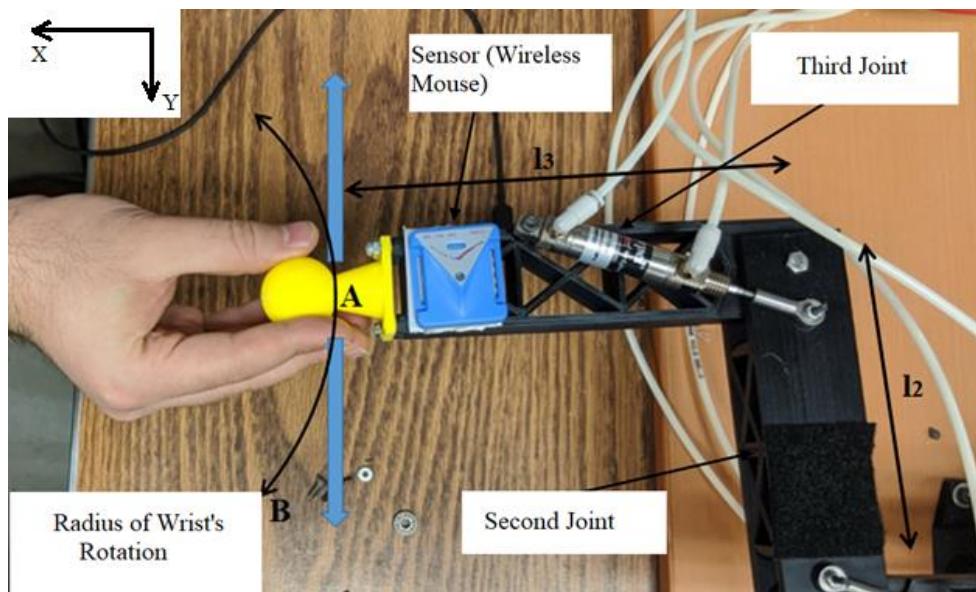
Figure 6-1. Second and third joint of manipulandum

Since the motion here is in XY plane, all Z coordinates will be negated. The last two joints of the robot in Figure 6-1 can be simplified as Figure 6-2. From the previous chapter we know that: $l_2=143\ mm$, $l_3=154\ mm$.
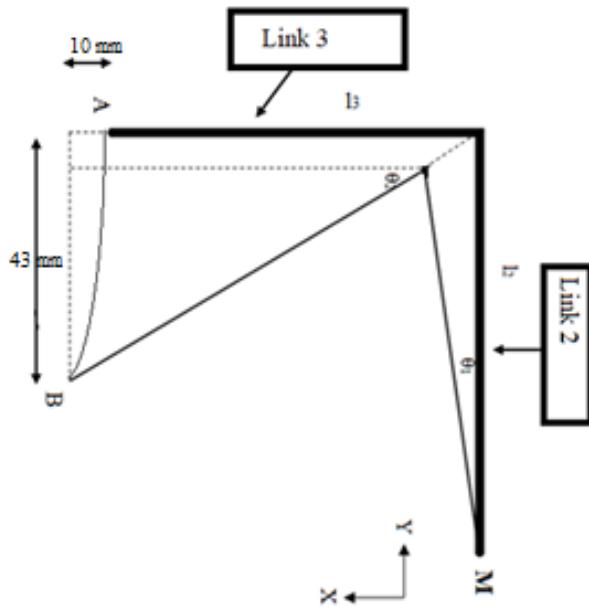

Figure 6-2. 2D top view of final prototype for second and third joint

The location of point A with respect to point M is A (l_3, l_2) = (154 mm,143 mm). From the experiment and by choosing the point B at the location (164 mm,100 mm).

From Figure 6-2, X_B and Y_B can be calculated as follows:

$$X_B = l_3 + l_2 s\theta_1 \tag{6.0}$$

$$Y_B = l_2 - l_3 s\theta_2 \tag{6.1}$$

By substituting point B in the equations (6.0) and (6.1) we get:

$$\theta_1 = 3.6 \text{ (deg)}$$

$$\theta_2 = 16 \text{ (deg)}$$

To summarise, if the hand is attached to the end point of the end-effector, by rotating the hand clockwise or counter-clockwise, the third joint will be moving the most, and the other joints will be barely moving. In other words, when rotating the manipulandum horizontally, the third joint will be rotating symmetrically to the wrist, the rotation of the second joint will be negated, and the first joint does not rotate in the XY plane.

The purpose of this section is to validate that the separate data obtained from both sensors (wrist sensor and robot sensor) as shown in Figure 6-3 and Figure 6-4 represent or match each other. The goal is to prove that the sensor attached to the robot is reading the same values as the one attached to the wrist. To prove this, it will be demonstrated that both are moving towards the same direction. The forearm will be locked using the other hand. The radius of the wrist rotation is smaller than the robot's rotation. The data coming from the wireless mouse mounted on the end of the fingers (to get a larger radius of rotation) should be in agreement with the one mounted on the robot, but the range of the motion should be smaller.
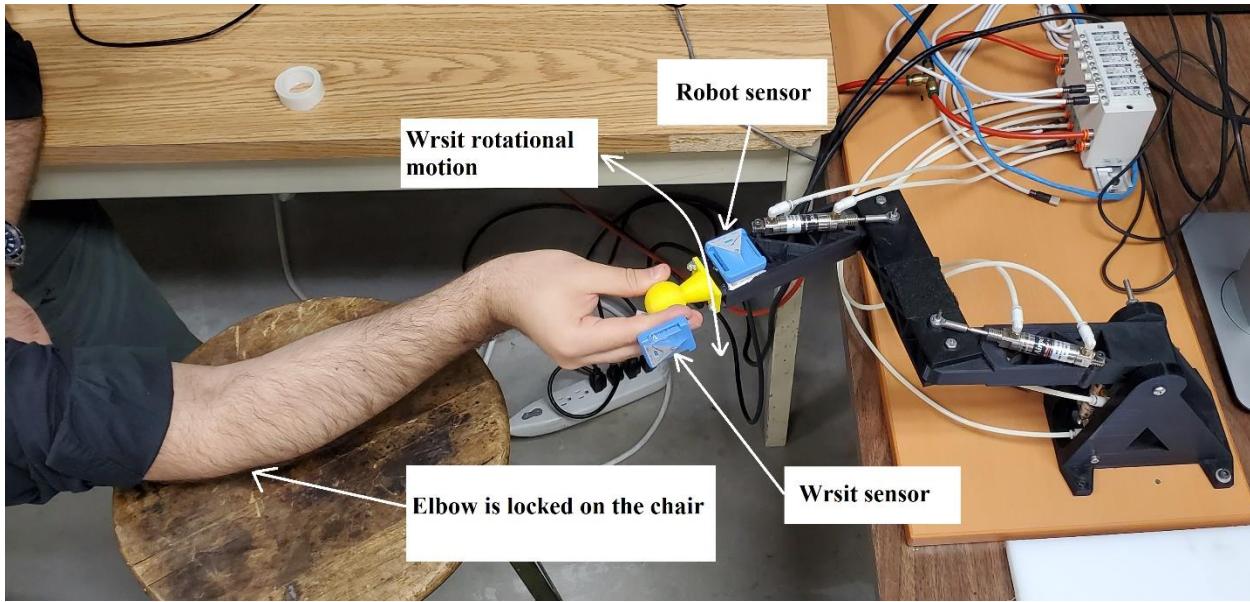
Figure 6-3. Wrist position for flexion and extension motion
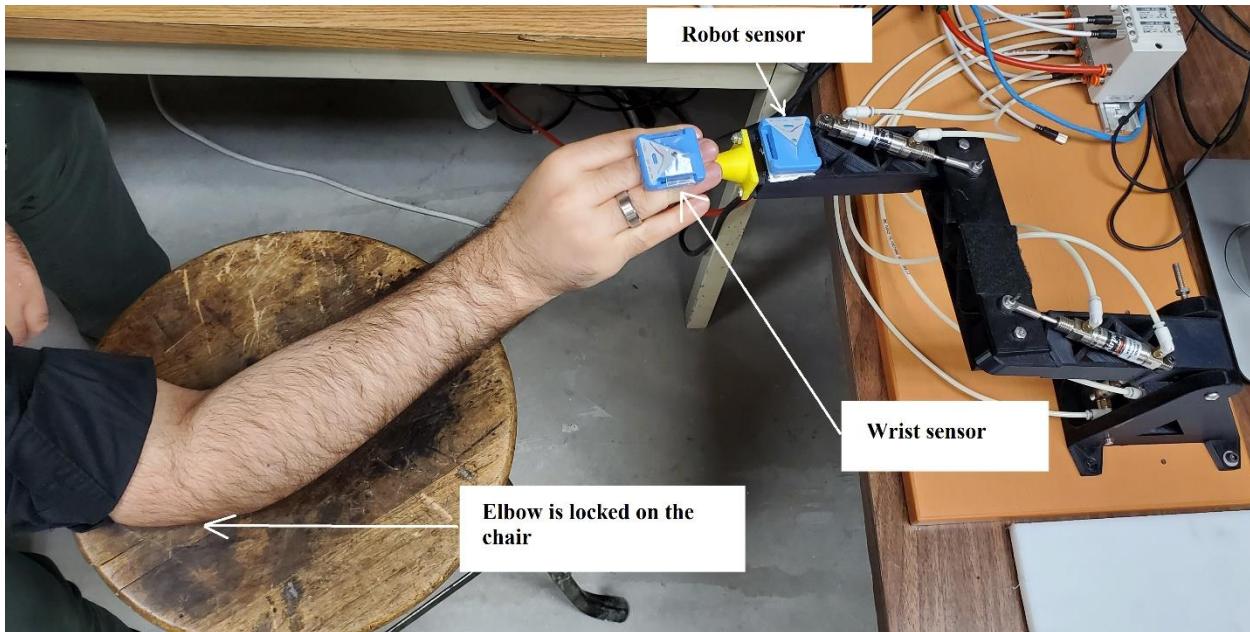
Figure 6-4. Wrist position for ulnar deviation and radial deviation motion

Since the sensor is a wireless mouse, and only one mouse can be connected to a PC, each of the two sensors will be connected to a different PC. The experiment is to run both at the same time for 3 seconds before moving the robot left and right using only the wrist. Finally, the data obtained

from the experiment will be compared. Since the robot is moving only in one axis, the data will be only the movement along the X-axis of the screen for 3 seconds.

The wireless mice move in a rotating motion, this motion translates into a linear motion that moves horizontally in the X-axis and vertically in the Y-axis of the computer's screen.

By comparing Figures 6-5 and Figure 6-6 we can observe that both figures have the same pattern, behaviour, direction and reverse direction. This proves that the robot is matching the motion of the wrist.
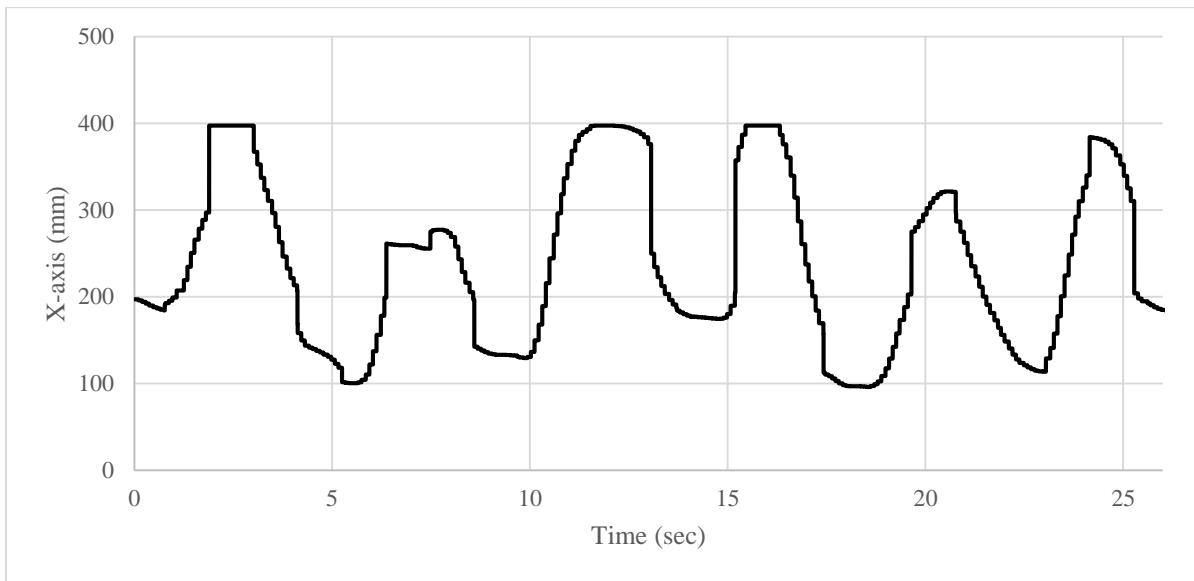

Figure 6-5. Data from sensor installed on the hand to represent wrist motion
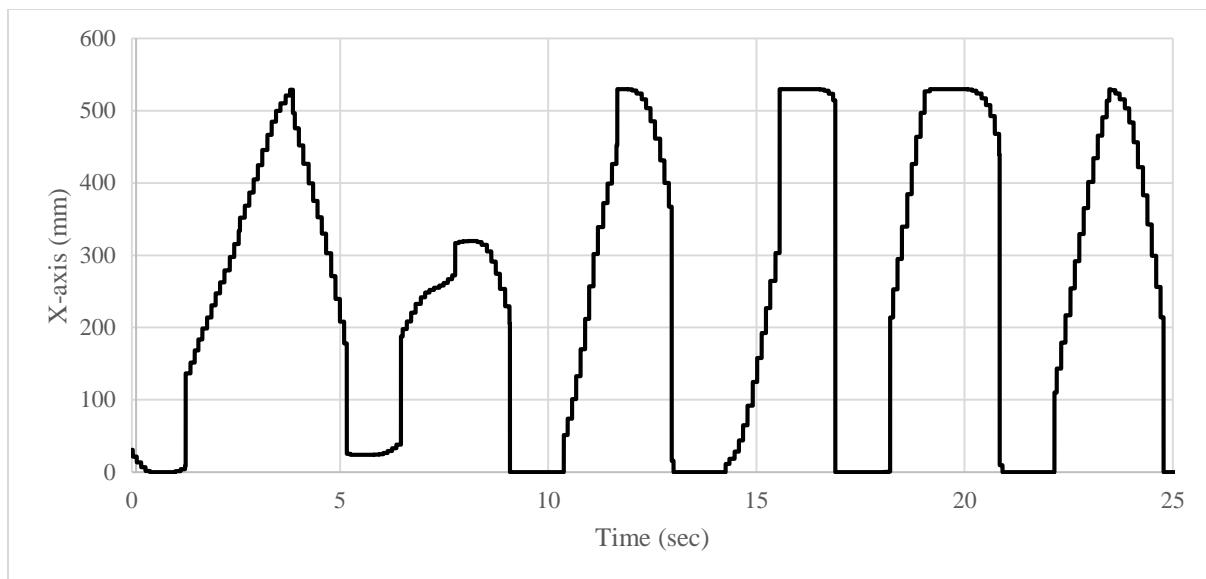
Figure 6-6. Data from sensor installed on manipulandum

The X-axis in both Figures (Figure 6-5 and Figure 6-6) represent the displacements of the mouse

pointer in the computer's screen.

6.2. Experimental results

In this section, data will be collected from the experiments using two methods. The first method is using image processing, the second method is using serial port. Each method will run in three different modes (assistive mode, resistive mode, and assistive with hysteresis mode).

6.2.1. Image processing method

The software uses image processing to read the position of the ball and the paddle by taking three screenshots of the game's screen (game in Figure 5-8) every one second. Depending on the difference in location of the paddle and the ball in the X-axis, the manipulandum will assist or resist the patient's movements, depending on the mode used in the experiment. These modes are discussed as follows:

Assistive mode

The goal of this mode is to assist the patient to move the paddle toward the ball. Figures 40 and 41 illustrate the extent pressure, the retract pressure and the error over time. For example, at the second 26, the error is at the max value on the negative side at -0.4. From the code we have:

$$\text{Error} = \text{Target} - \text{Paddle} \qquad\qquad 6.1$$

(-0.4) which means that the paddle is at the max right of the screen, and the ball is at the farthest left of the screen. In this situation the controller will send two command signals, one to close the control valve that will activate the retract pressure, and another to open the control valve that will activate the extent pressure. From Figures 6-7, 6-8 and 6-9, we can see that the value of the pressure is proportional to the value of the error. This means that the pressure will be higher if the error is increasing and will be lower if the paddle is going towards the ball.

From Figure 6-9 at the seconds [26 to 27] the value of the error is at the maximum value at the negative side (-0.4), the objective of the robot in this situation is to assist the patient to move the paddle toward the ball. Since the value of the error is maxed, the value of the extent pressure is maxed at 100 (psi) (shown in Figure 6-7). However, the value of the retract pressure is zero (shown in Figure 6-8). Also, from the seconds [22 to 25] the value of the error (Figure 6-9) is dropping from [0.4 to 0] and the retract pressure (Figure 6-8) is assisting the patient to move the paddle to the target.
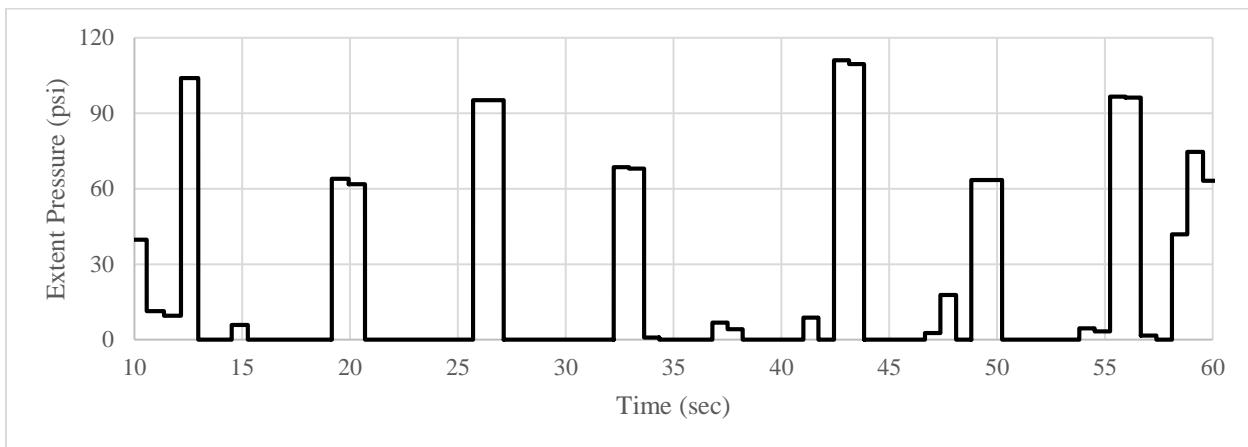

Figure 6-7. Extent pressure of assistive mode
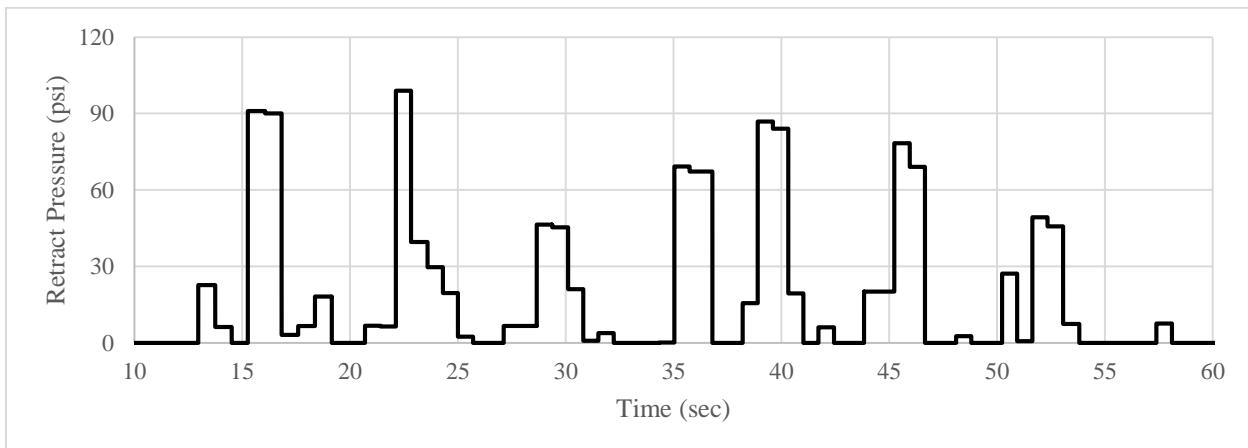
Figure 6-8. Retract pressure of assistive mode
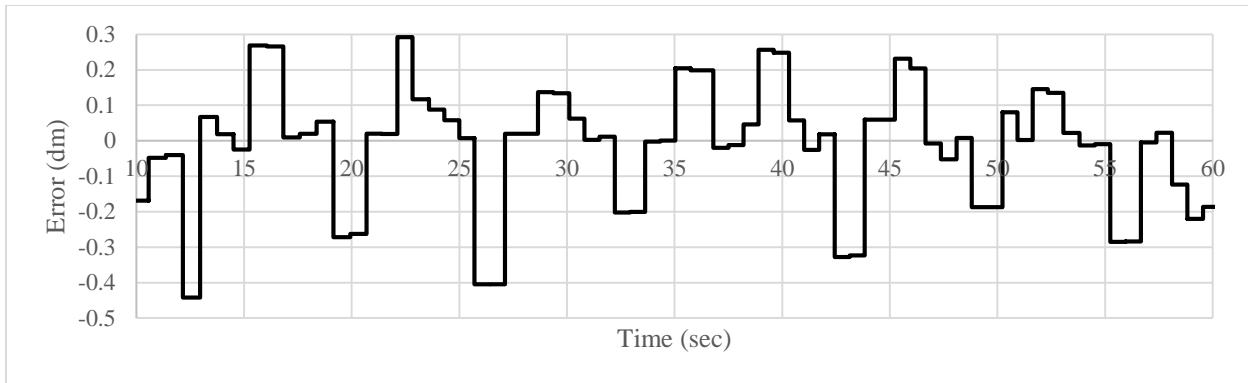
Figure 6-9. Error over time of assistive mode
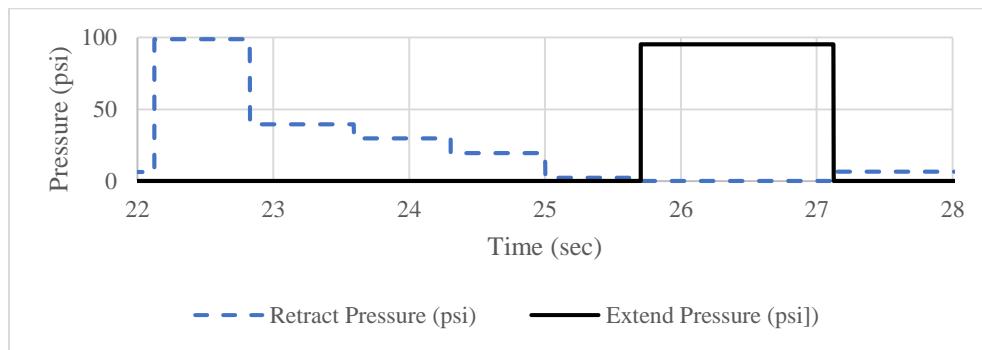
Figure 6-10. Values of extent and retract pressure from 22-28 second
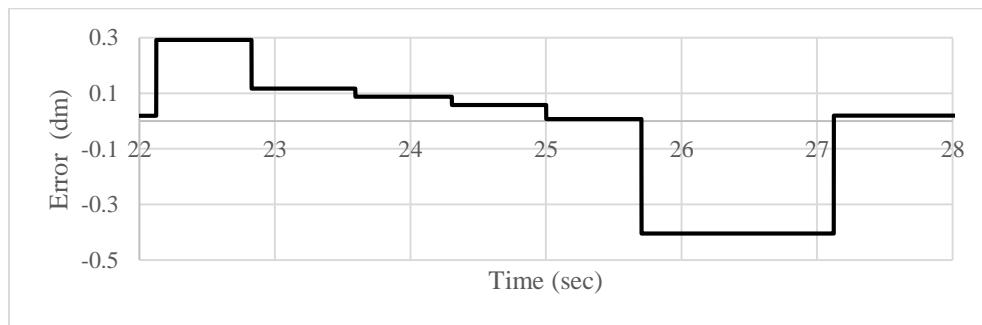
Figure 6-11. Value of error over time from 22-28 second

Figure 6-10 represents the value of the extent pressure and the retract pressure shown in Figures 6-7 and 6-8 from the seconds [22 to 28]. Figure 6-11 represent the value of the error shown in Figure 6-9 for the same time.

61

Resistive mode

The resistive mode is the opposite of the assistive mode, the goal of this mode is to prevent the patient from moving the paddle toward the ball. From Figure 6-14 second [21 to 24], the value of the error is decreasing, which means the paddle is heading towards the ball, which can be seen in Figure 6-12. At the same time from second [22 to 25] the value of the extent pressure is increasing from 0 (psi) to 80 (psi) to resist the patient. However, the value of the retract pressure (shown in Figure 6-13) is dropping to zero. From the second [25 to 27] the value of the error is decreasing from [-0.4 to 0] (the negative sign is to show that the ball is at the left side of the paddle) as noticed from Figure 6-13 the value of the retract pressure for the same range is increasing from (0 to 90) (psi), while the value of the extent pressure is dropping to zero.
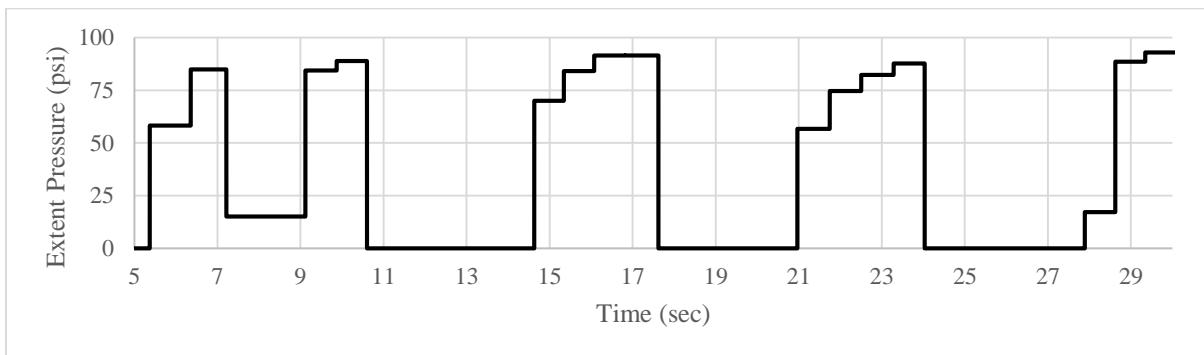

Figure 6-12. Extent pressure of resistive mode
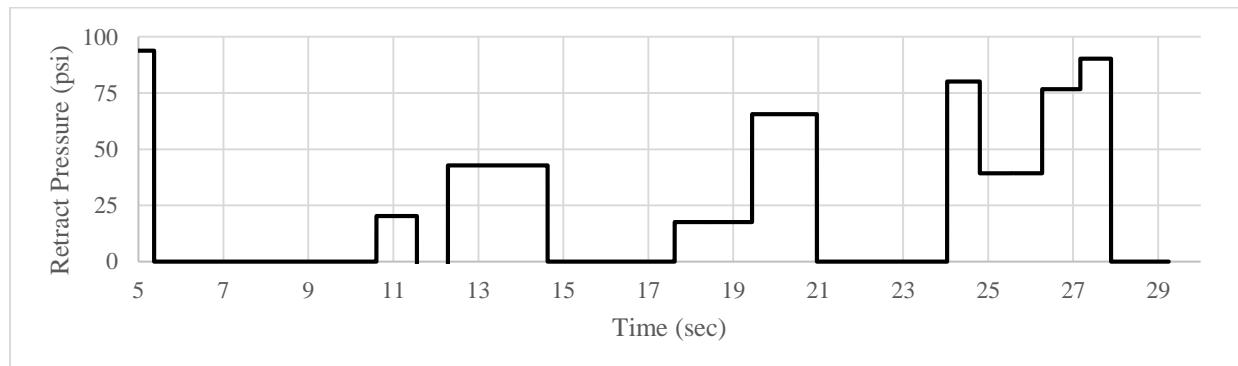
Figure 6-13. Figure 6 13. Retract pressure of resistive mode

62
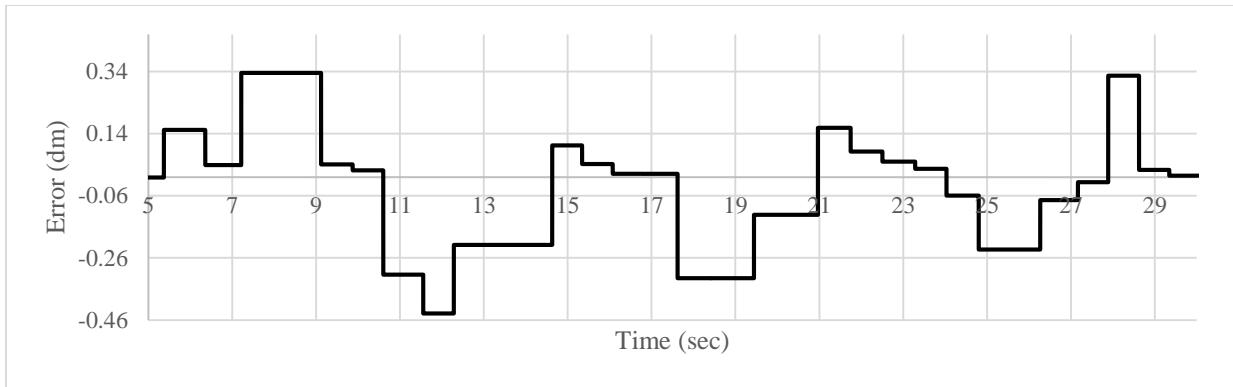
Figure 6-14. Error over time of resistive mode
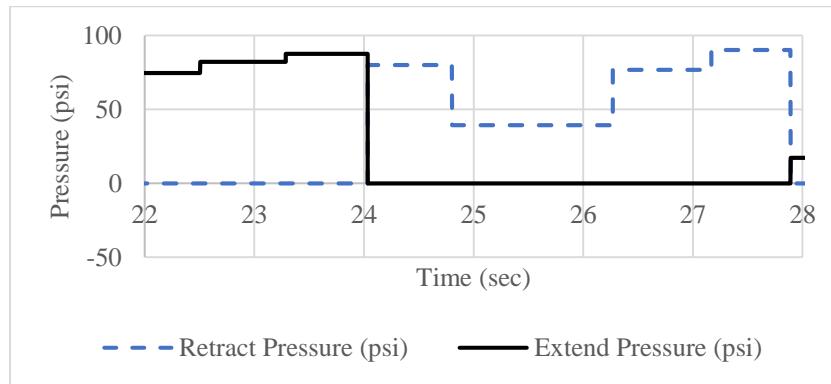
Figure 6-15. Values of extent and retract pressure from 22-28 second
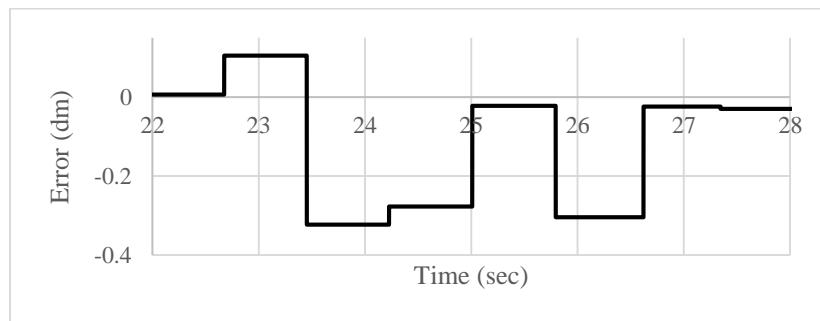
Figure 6-16. Values of extent and retract pressure from 22-28 second

Figure 6-15 represents the value of the extent pressure and the retract pressure shown in Figures 6-12 and 6-13 from the seconds [22 to 28]. Figure 6-16 represent the value of error shown in Figure 6-14 for the same time.

Assistive mode with hysteresis

In this mode, the manipulandum should only assist the patient for a certain value, where the error is greater than |0.2| and will do nothing when the value of the error is less than |0.2|. From Figures 6-17, 6-18 and 6-19, from the second [32 to 40] where the value of the error is changing within the values [-0.2 and 0.2], the value of the extent pressure and retract pressure is zero. Pressure will be applied anytime the value of the error is greater than |0.2|.
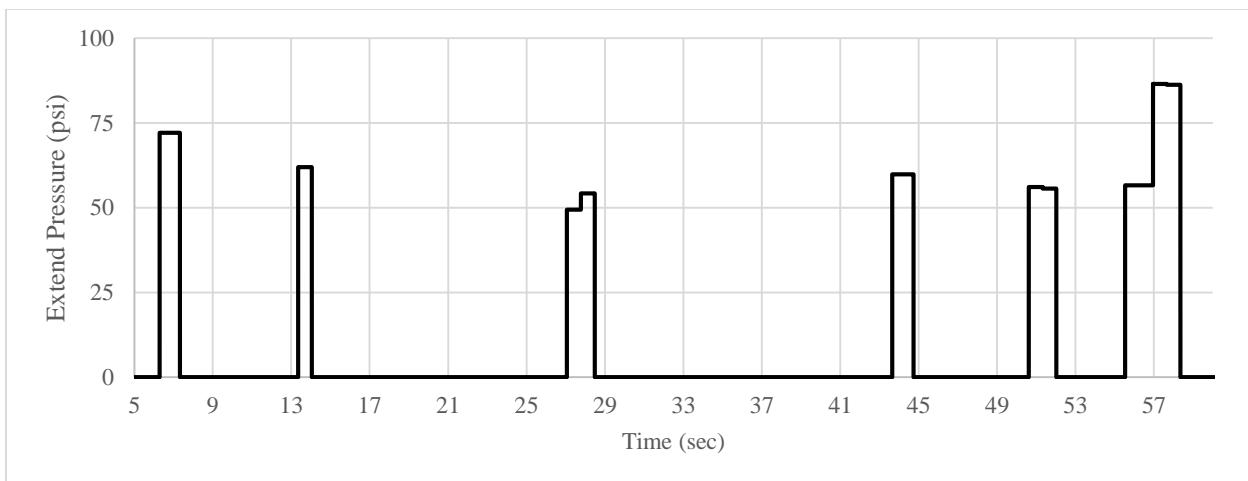
Figure 6-17. Extent pressure of assistive with hysteresis mode
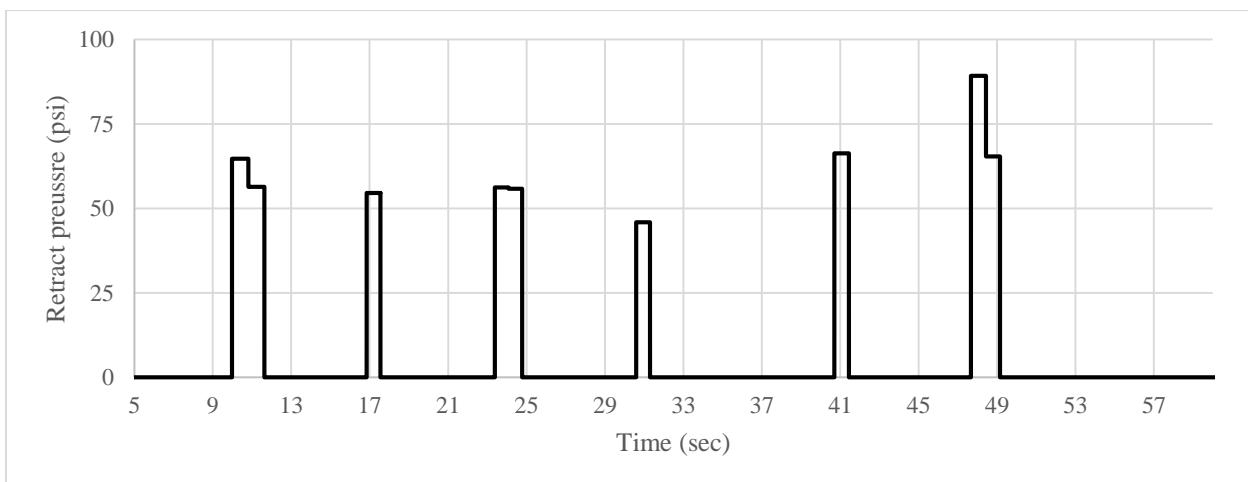
Figure 6-18. Retract pressure of assistive with hysteresis mode

64
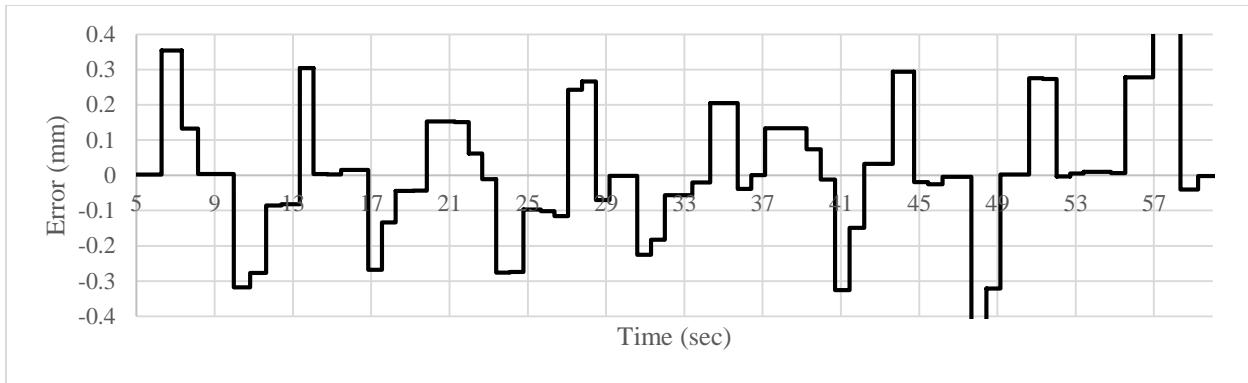
Figure 6-19. Error over time of assistive mode with hysteresis
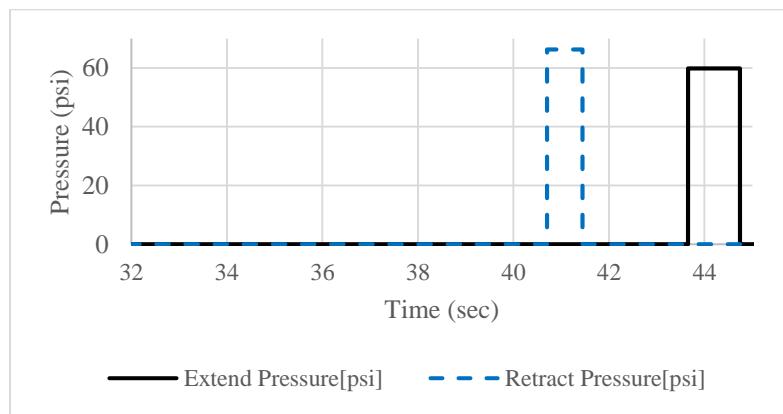
Figure 6-20. Values of extent and retract pressure from 32-45 second
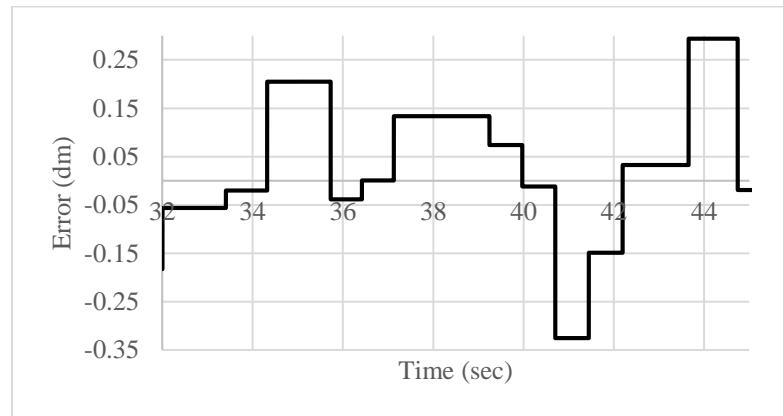
Figure 6-21. Values of error over time from 32-45 second

Figure 6-20 represents the value of the extent pressure and the retract pressure shown in Figures 6-17 and 6-18 from the seconds [32 to 45]. Figure 6-21 represent the value of error shown in Figure 6-19 for the same time.

6.2.2. File streaming method

At this stage, the software uses file streaming to read the position of the ball and the paddle, depending on the difference in location of each one it will either assist or resist the patient (depending on the mode being used in the experiment). This method allows us to get more data points per second. The file streaming method will provide the controller with 1000 data point per second while the image processing method only provides the controller with 3 data point per second. It is analysed using the same modes, which are discussed as follows:

Assistive mode

The goal of this mode is to assist the patient to move the paddle towards the ball. Figures 6-16 and 6-17 shows the extent pressure, the retract pressure and the error over time. In this method the error will be changing from (-1 to 1). So (-1) means that the paddle is at the max right of the screen, and the ball is at the farthest left of the screen. As before when the error is equal to (-1) the controller will send two command signals, one to deactivate retract pressure, and another one to activate the extent pressure. From Figures 6-22, 6-23 and 6-24, we can see that the value of the pressure is proportional to the value of the error. This means that the pressure will be maxed at the max value of the |error| and get lower when the value of the |error| is decreasing to zero.

From Figure 6-24 at the seconds [0 to 5] the value of the error is going from the maximum value (1 to 0). The manipulandum in this mode will assist the patient to move the paddle towards the ball. Since the value of the error is maxed, the value of the extent pressure is also maxed at 100 (psi) at second (0) (shown in Figure 6-22). However, the value of the retract pressure is zero (shown in Figure 6-23). Also, from the seconds [16 to 19] the value of the error (Figure 6-24) is fluctuating between [0 and -0.5] and the retract pressure (Figure 6-23) is also fluctuating between

[0 to 60] (psi) to assist the patient to move the paddle to the target, while the value of the extent pressure is equal to zero.
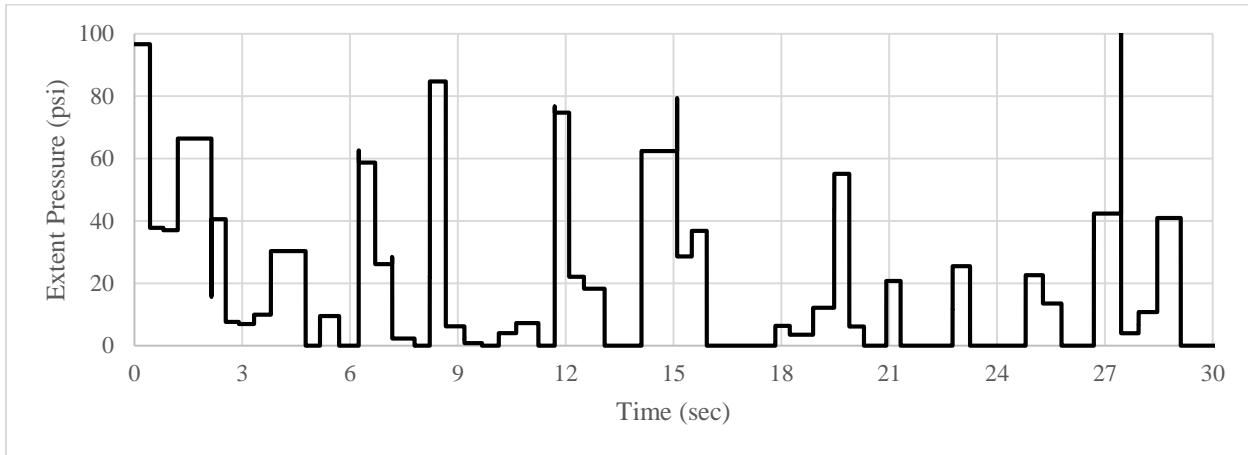
Figure 6-22. Extent pressure of assistive mode using file streaming method
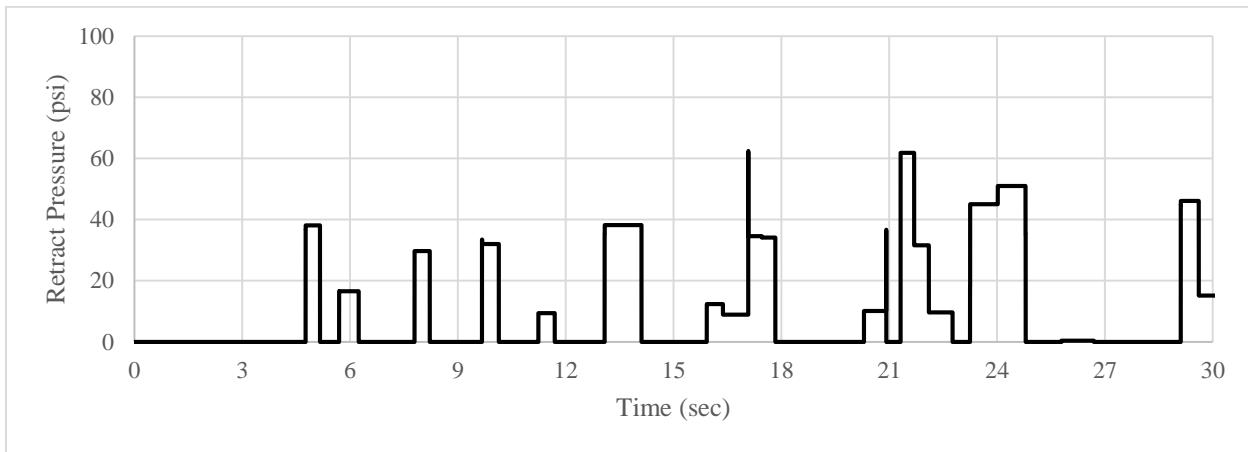


Figure 6-23. Retract pressure of assistive mode using file streaming method
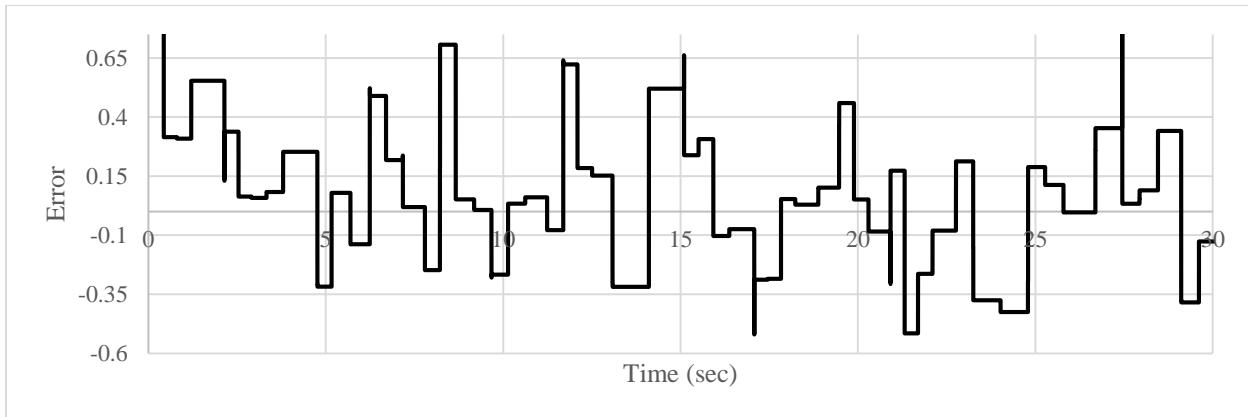
Figure 6-24. Error over time of assistive mode using file streaming method
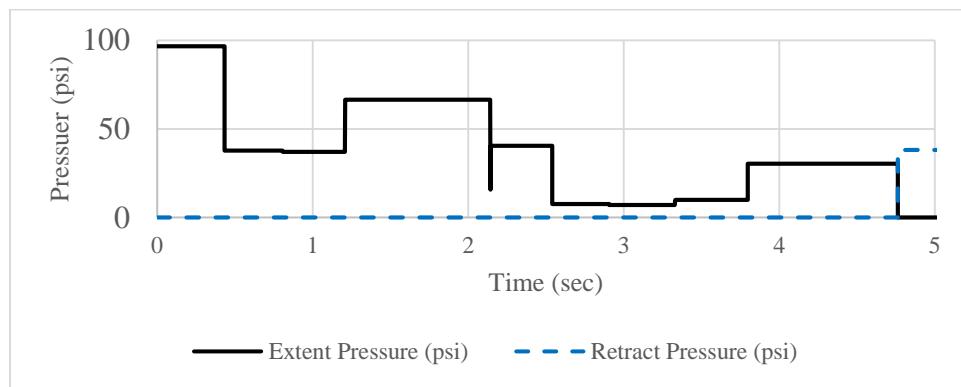
Figure 6-25. Values of extent and retract pressure from 0-5 second
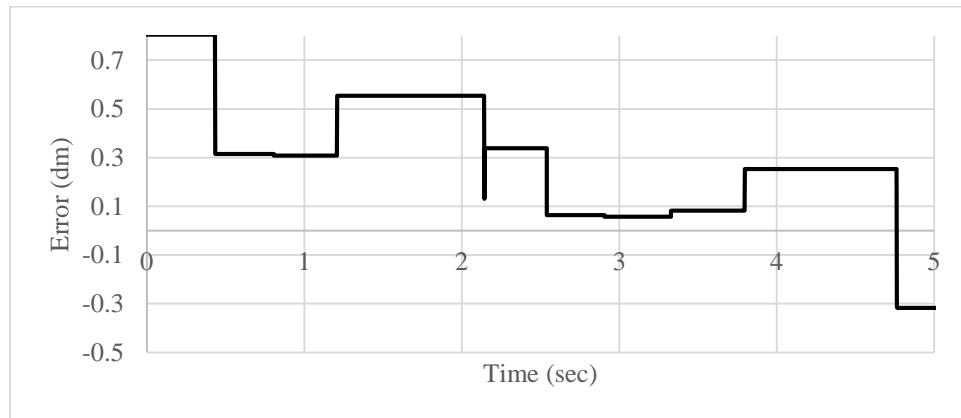
Figure 6-26. Values of error over time from 0-5 second

Figure 6-25 represents the value of the extent pressure and the retract pressure shown in Figures

6-22 and 6-23 from the seconds [0 to 5]. Figure 6-26 represent the value of error shown in Figure

6-24 for the same time.

Resistive mode

The manipulandum here intentionally prevents the patient from moving the paddle towards the ball. As shown in Figure 6-29 second [6 to 10], the value of the |error| is decreasing, which means the paddle is heading towards the ball, as noticed in Figure 6-27 for the same at the same time from second [6 to 10] the value of the extent pressure is increasing from 0 to 80 (psi) to act as a resistive force against the patient. However, the value of the retract pressure (shown in Figure 6-28) is zero.

Also, from the second [14 to 16] the value of the |error| is also decreasing from [-0.5 to 0] (the negative sign is to show that ball is at the left side of the paddle). As can be seen in Figure 6-28 the value of the retract pressure for the same range of time is increasing from (0 to 70) (psi), while the value of the extent pressure is zero.
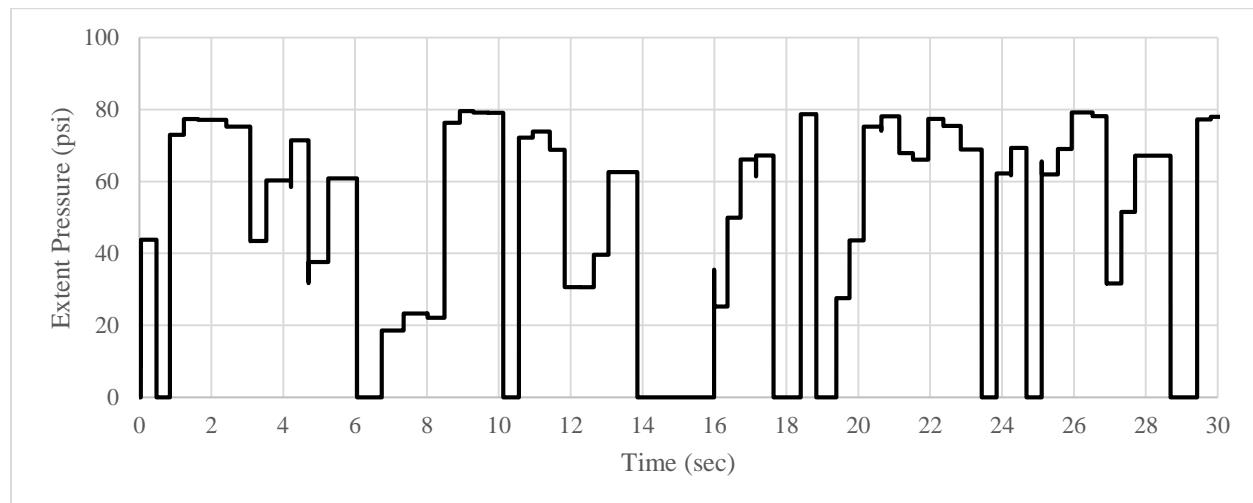

Figure 6-27. Extent pressure of resistive mode using file streaming method
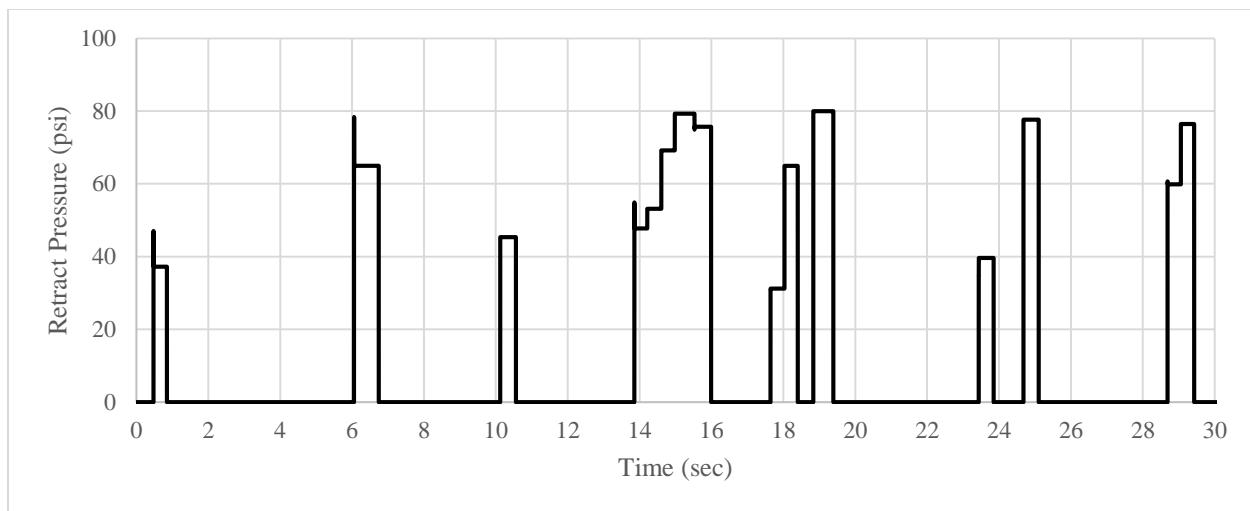
Figure 6-28. Retract pressure of resistive mode using file streaming method
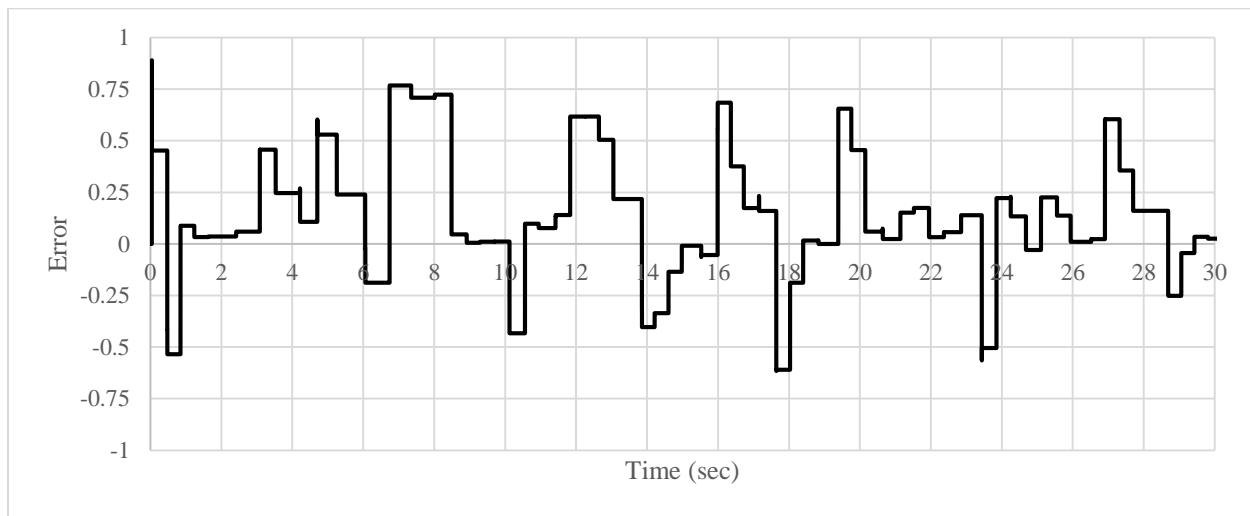

Figure 6-29. Error over time of resistive mode using file streaming method
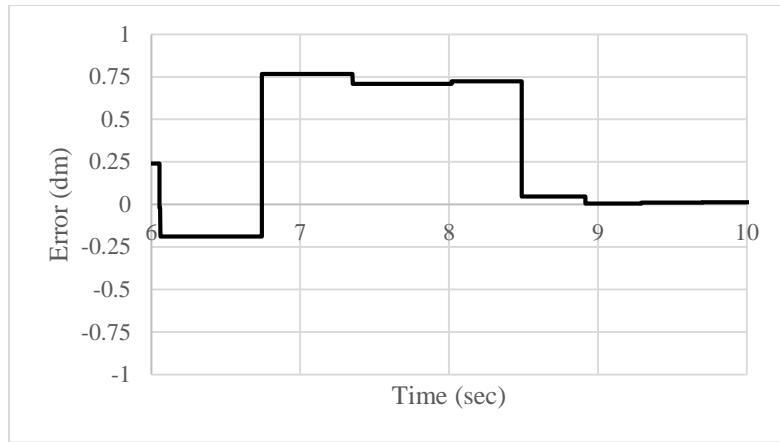
Figure 6-30. Values of extent and retract pressure from 6-10 second
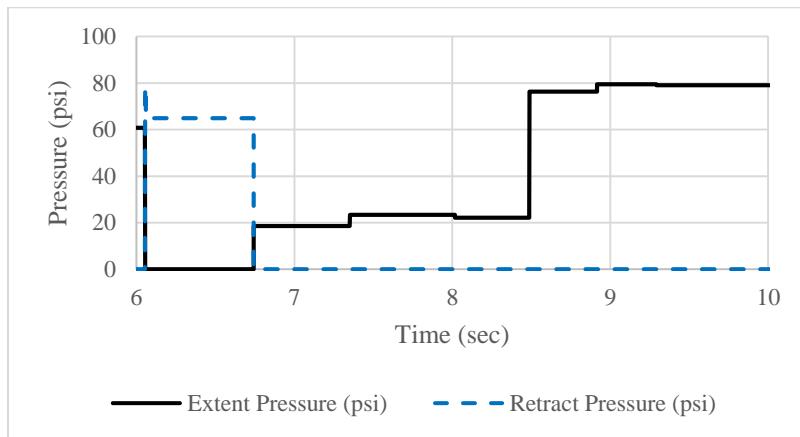
Figure 6-31. Values of error over time from 6-10 second

Figure 6-30 represents the value of the extent pressure and the retract pressure shown in Figures 6-27 and 6-28 from the seconds [0 to 5]. Figure 6-31 represent the value of error shown in Figure 6-29 for the same time.

Assistive mode with hysteresis

In this mode, the manipulandum is only to assist the patient for a certain value, where the error is greater than |0.3|, and will do nothing when the value of the error is less than |0.3|. From Figures 6-32, 6-33 and 6-34, from the second [5 to 10] where the value of the error is changing within the values [-0.3 and 0.3] the value of the extent pressure and retract pressure is zero. Pressure will be applied anytime the value of the error is greater than |0.3|.
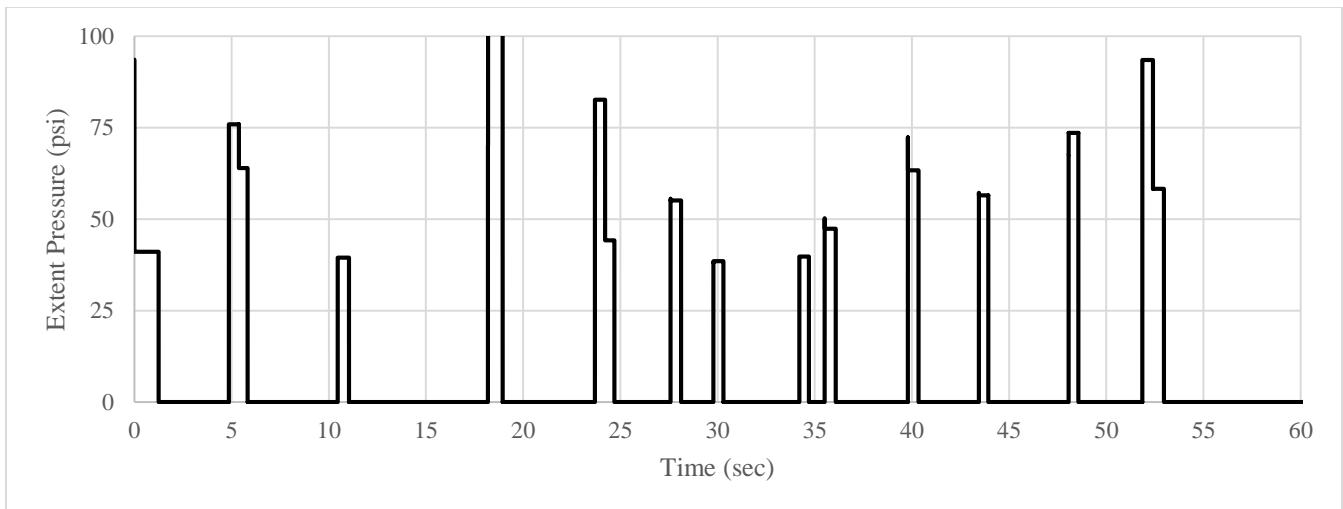

Figure 6-32. Extent pressure of assistive mode using file streaming method
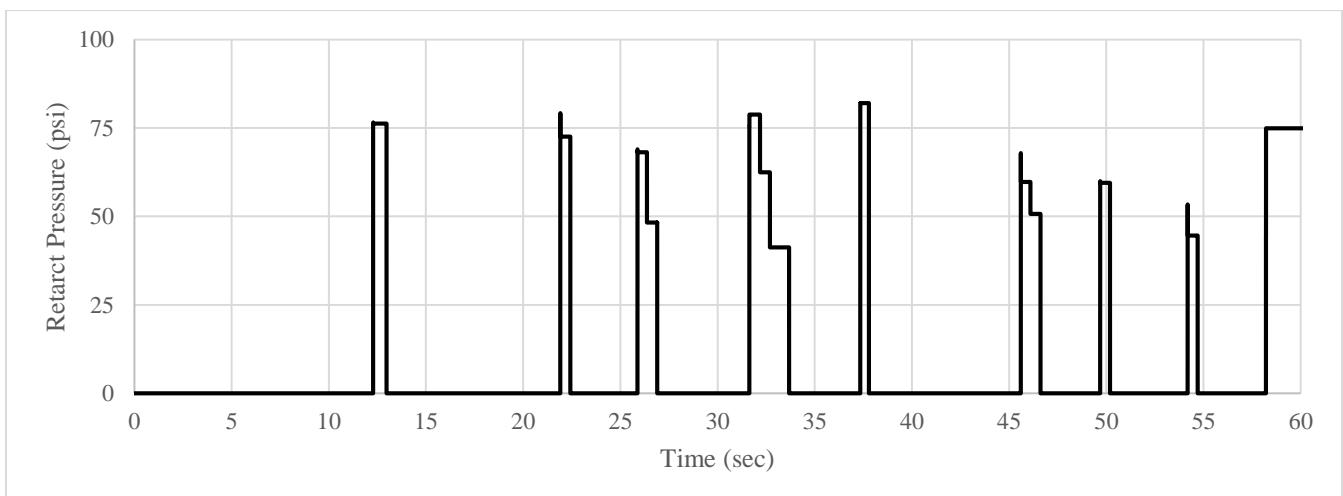
Figure 6-33. Extent pressure of assistive mode using file streaming method
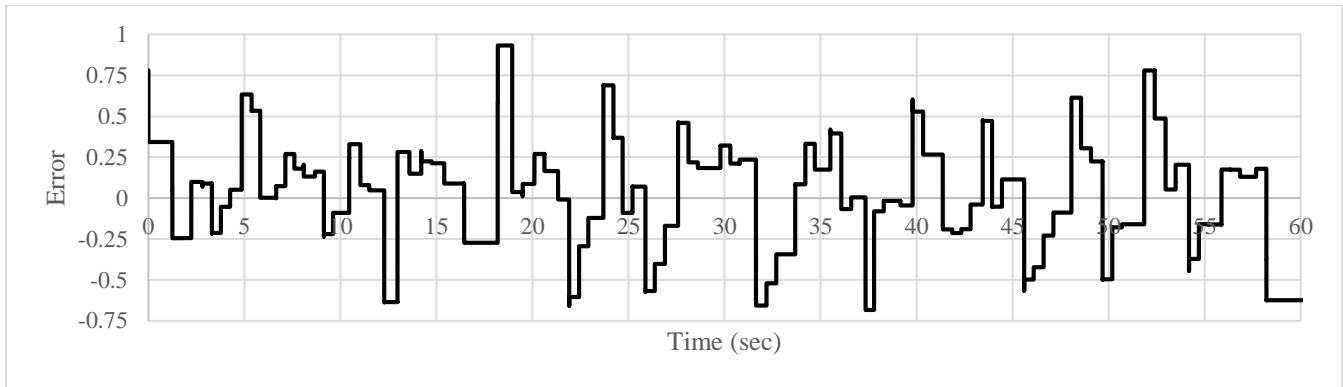
Figure 6-34. Error over time of assistive mode using file streaming method
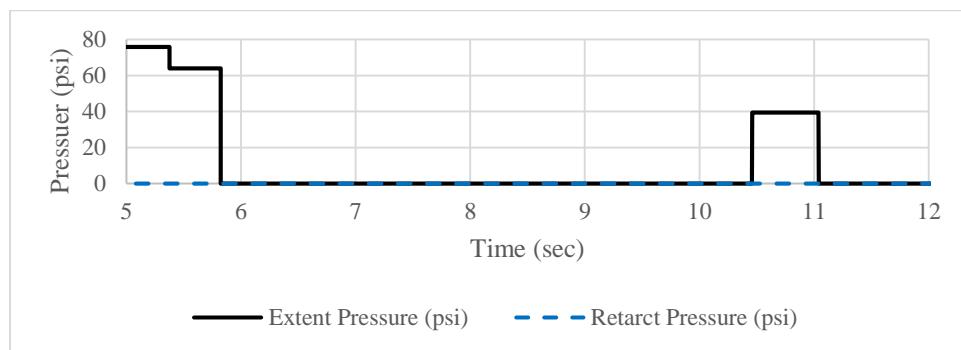
Figure 6-35. Values of extent and retract pressure from 5-12 second
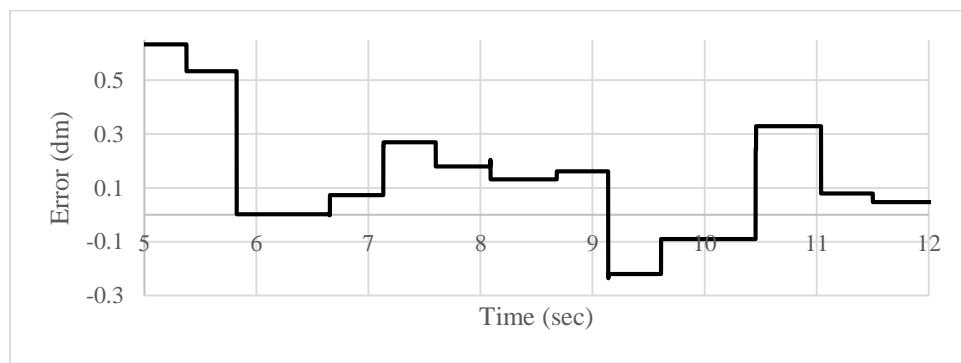

Figure 6-36. Values of error over time from 5-12 second

Figure 6-30 represents the value of the extent pressure and the retract pressure shown in Figures 6-27 and 6-28 from the seconds [0 to 5]. Figure 6-31 represent the value of error shown in Figure 6-29 for the same time.

6.3.   Summary and discussions

This chapter provided analysis of the third joint to match the wrist motion (ulnar deviation and radial deviation, flexion and extension). The data from the robot sensor was then validated to match the data on the sensor attached to the wrist. Moreover, the three modes (assistive, resistive, and assistive with hysteresis) were run and analyzed in two different methods: image processing and file streaming. Both methods proved to work in the three modes, since the game is a 2D basic game and there are only two things to measure (ball position and paddle position). File streaming proved to be more accurate than image processing, for the following reasons: firstly, it provides more data points per second and takes less time to compile and execute the code. Each data point reads ball position, paddle position and writes an error value, extent pressure value and retract pressure value. The image processing method provided 3 data points per second while the file streaming method provided 1000 data points per second. Alongside this, while using the image processing method the manipulandum had a delay of one (sec) behind because it takes more processing time, the delay in the file streaming method was lower (less than 0.2 sec behind). This time can further be improved when using the file streaming method by taking less data points per second.

Secondly, the image processing method proved to work in only one situation, where the ball is falling in a straight trajectory. Contrastingly, the file streaming method proved to work in all situations where the ball goes in a non-linear motion while falling since it updates its data every 1(ms).

Thirdly, the assistive mode when required could not be tested using the image processing method because of the very low number of the data points per second. This prevents the acquirement of the derivative for the error. Furthermore, even if the derivative could be acquired there would be

a two second delay, which would disrupt the rest of the experiment since there is a new ball falling

every 1.5 (sec).

7. Conclusions

7.1. Contributions made in this thesis

This thesis set out to provide the design of a manipulandum device that can serve as a robot-assisted rehabilitation device for wrist rehabilitation. It was successful in delivering the design of a device that: consists of cost-effective components, is capable of both assisting and resisting the movement of a patient's wrist in two directions and can be made using fMRI compatible materials. The device designed in this thesis was also successful in its ability to increase the interactivity and enjoyment of a patient's treatment using an interactive game. The game not only benefits patients by increasing their desire to partake in rehabilitation exercises, but it can also provide valuable data to health care providers.

To achieve this, a 3 DOF pneumatic manipulandum device was designed and prototyped for wrist rehabilitation. The geometrics of the manipulandum were designed based on the following requirements: the workspace for every arm should be symmetrical with respect to the horizontal plane and the chosen actuator has to generate force that overcomes the minimum required force while meeting the geometrical constraints. The workspace and the necessary force were analyzed based on the kinematics of the manipulandum. This device was constructed based on three previously developed prototypes.

The new prototype improved the design and characteristics of these previous devices in a number of ways. Firstly, the final prototype is made from thermoplastic, which is cheaper and lighter than aluminum and acrylic. Secondly, this device possessed a larger workspace in the XY plane which allow for a greater range of movements for the patient at 120 (mm) of wrist rotation and could compensate for the required forces with an actuator force of 10 (N). Thirdly, the pneumatic

actuators that were used for the final design of the devices are commercially available from non-magnetic material, which can be used in an fMRI environment. Fourthly, the decreased DOF from previous devices (only using 3) allows for simpler and more efficient control of the device as well as faster execution of its code. Finally, the interactive game allowed for a more engaging form of treatment that can record quantitative data.

The performance of the manipulandum designed in this thesis was analyzed using two methods; image processing and file streaming. Through conducting experiments, it was shown that file streaming proved to be the most reliable and accurate method. The results of the experiments demonstrate that the image processing method provided 3 data points per second, while the file streaming method provided 1000 data points per second. Furthermore, the file streaming method proved to be functional with more modes, notably assistive mode when required. The assistive mode when required needs more data point per second than the image processing method can provide, since the assistive mode when required needs the derivative of the error over time.

7.2. Future work

The device created was successful in achieving the proposed objectives of the thesis. These objectives:

- A cost-effective device that can be used as a substitute form of treatment in rehabilitation.

- A device that provides force-feedback that is capable of accommodating movement of the wrist in any direction.

- A device that provides a platform that is capable of both assisting and resisting three motions of the wrist.

- A device that is available in fMRI-compatible material to support fMRI studies.

Improvements can be made to further increase the capabilities of the device. These improvements include:

- The 3 DOF of the device can be used in conjunction with more mechanically complicated games, which allow for more wrist motions (Ulnar Deviation, the Radial Deviation, Flexion and the Extension) at the same time, rather than doing them separately one by one.

- All parts used in the device including bolts, nuts, ball bearings, wireless mice and actuators are available in a non-magnetic material. Therefore, a non-magnetic version of the device can be made for fMRI studies.

- Many improvements can be made in the software architecture of the game itself, which will allow for reduced the compiling time of its code and execution.

- Delay time resulting from image processing method can be improved by using two computers, one can do the image processing analysis by using a camera and send the data to the other one, which does the control part.

References

[1] National Institute of Neurological Disorders and Stroke, "Post-Stroke Rehabilitation Fact Sheet," *National Institute of Neurological Disorders and Stroke*. [Online]. Available: https://www.ninds.nih.gov/Disorders/Patient-Caregiver-Education/Fact-Sheets/Post-Stroke-Rehabilitation-Fact-Sheet. [Accessed: Dec 23, 2019].

[2] V. Y. Ma, L. Chan, and K. J. Carruthers, "Incidence, Prevalence, Costs, and Impact on Disability of Common Conditions Requiring Rehabilitation in the United States: Stroke, Spinal Cord Injury, Traumatic Brain Injury, Multiple Sclerosis, Osteoarthritis, Rheumatoid Arthritis, Limb Loss, and Back Pain," *Archives of Physical Medicine and Rehabilitation*, vol. 95, no. 5, pp. 986–995, 2014.

[3] J. M. Bertolote, "Neurological disorders affect millions globally: WHO report," World Neurology 22, no. 1, 27 Feb. 2007

[4] M. Babaiasl, S. H. Mahdioun, P. Jaryani, and M. Yazdani, "A review of technological and clinical aspects of robot-aided rehabilitation of upper-extremity after stroke," *Disability and Rehabilitation: Assistive Technology*, vol. 11, no. 4, pp. 263–280, 2015.

[5] C. Basdogan, S. D. Rensselaer, J. Kim, M. Muniyandi, H. Kim, and M. Srinivasan, "Haptic rendering - beyond visual computing - Haptics in minimally invasive surgical simulation and training," *IEEE Computer Graphics and Applications*, vol. 24, no. 2, pp. 56–64, Mar. 2004.

[6] National Institute of Biomedical Imaging and Bioengineering, "Magnetic Resonance Imaging (MRI)," *National Institute of Biomedical Imaging and Bioengineering*. [Online]. Available: https://www.nibib.nih.gov/science-education/science-topics/magnetic-resonance-imaging-mri. [Accessed: Mar 22, 2019].

[7] B. Yang, U.-X. Tan, A. B. McMillan, R. Gullapalli, and J. P. Desai, "Design and Control of a 1-DOF MRI-Compatible Pneumatically Actuated Robot with Long Transmission Lines," *IEEEASME Trans. Mechatron.*, vol. 16, no. 6, pp. 1040–1048, Dec. 2011.

[8] J. Erwin and M. Varacallo, "Anatomy, Shoulder and Upper Limb, Wrist Joint.", *StatPearls [Internet]*, Treasure Island (FL): StatPearls Publishing LLC, 2020. [E-book] Available: ncbi.nlm.nih.gov

[9] Dictionary, [Online], Available: http://dictionary.reference.com/browse/haptic, [Accessed March 11, 2010]

[10] H. S. Kim, "Kinematically Redundant Parallel Haptic Device with Large Workspace," *International Journal of Advanced Robotic Systems*, vol. 9, no. 6, p. 260, 2012.

[11] R. E. Sofronia, G. Savii, and A. Davidescu, "Haptic devices in engineering and medicine," 2010 *IEEE International Joint Conference on Computational Cybernetics and Technical Informatics*, 2010, pp. 373–378,

[12] J. S. Thomas, D. A. Croft, and V. B. Brooks, "A Manipulandum for Human Motor Studies," *IEEE Transactions on Biomedical Engineering*, vol. BME-23, no. 1, pp. 83–84, 1976.

[13] W. Gezari, and D. Y. Gezari. "Muscle exercise and/or rehabilitation apparatus using linear motion." U.S. Patent 4,907,797, issued March 13, 1990.

[14] J. Izawa, T. Shimizu, H. Gomi, S. Toyama, and K. Ito, "MR compatible manipulandum with ultrasonic motor for fMRI studies," In Proc. 2006 IEEE International Conference on Robotics and Automation, 2006. ICRA 2006., pp. 3850–3854, 2006.

[15] H.-K. Lee, Y.-T. Kim, Y. Takahashi, T. Miyoshi, K. Suzuki, and T. Komeda, "Basic Experiment on Rehabilitation of Upper-Limb Motor Function Using Haptic-Device System," *Transactions of the Korean Society of Mechanical Engineers A*, vol. 35, no. 5, pp. 459–467, 2011.

[16] B. Ghannadi, R. S. Razavian, and J. Mcphee, "Configuration-Dependent Optimal Impedance Control of an Upper Extremity Stroke Rehabilitation Manipulandum," *Frontiers in Robotics and AI*, vol. 5, p. 124, 2018.

[17] D. Chablat and P. Wenger, "The kinematic analysis of a symmetrical three-degree-of-freedom planar parallel manipulator," *arxiv.org*, June 2007. [Online], Available: https://arxiv.org/abs/0705.0959, [Accessed: January 2019]

[18] G. Campion, "The Pantograph Mk-II: A Haptic Instrument, *The Synthesis of Three Dimensional Haptic Textures: Geometry, Control, and Psychophysics*, pp. 45–58, London: Springer, 2005.

[19] L. Birglen, C. Gosselin, N. Pouliot, B. Monsarrat, and T. Laliberte, "SHaDe, a new 3-DOF haptic device," *IEEE Transactions on Robotics and Automation*, vol. 18, no. 2, pp. 166–175, 2002.

[20] M. R. Sirouspour, S. P. Dimaio, S. E. Salcudean, P. Abolmaesumi, and C. Jones, "Haptic interface control-design issues and experiments with a planar device," *Proceedings 2000*

ICRA. Millennium Conference. IEEE International Conference on Robotics and Automation. Symposia Proceedings (Cat. No.00CH37065), 2000, pp. 789–794.

[21]   L. Stocco, S. Salcudean, and F. Sassani, "Optimal kinematic design of a haptic pen," *IEEE/ASME Transactions on Mechatronics*, vol. 6, no. 3, pp. 210–220, 2001.

[22]   Y. Tsumaki, H. Naruse, D. Nenchev, and M. Uchiyama, "Design of a compact 6-DOF haptic interface," *Proceedings. 1998 IEEE International Conference on Robotics and Automation (Cat. No.98CH36146)*, 1998, pp. 2580–2585.

[23]   G. Long and C. Collins, "A pantograph linkage parallel platform master hand controller for force-reflection," *Proceedings 1992 IEEE International Conference on Robotics and Automation*, 1992, pp. 390–391.

[24]   F. Pierrot, C. Reynaud, and A. Fournier, "DELTA: a simple and efficient parallel robot," *Robotica*, vol. 8, no. 2, Apr, pp. 105–109, 1990.

[25]   S. Grange, F. Conti, P. Helmer, P. Rouiller, and C. Baur, "Delta Haptic Device as a nanomanipulator," *Microrobotics and Microassembly III*, vol. 4568, pp. 100–111, Oct. 2001.

[26]   W. K. Yoon, T. Seuhiro, Y. Tsumaki, M. Uchiyama, (2004), "Stiffness Analysis and Design of a Compact Modified Delta Parallel Mechanism," *Robotica,* vol. 22, pp. 463–475, Aug. 2004.

[27]   "Force   Dimension   –   products."   [Online] Available: http://www.forcedimension.com/products. [Accessed: August 17, 2017]

[28]   J. Fong, V. Crocher, Y. Tan, D. Oetomo, and I. Mareels, "EMU: A transparent 3D robotic manipulandum for upper-limb rehabilitation," *2017 International Conference on Rehabilitation Robotics (ICORR)*, pp. 771-776, Jul. 2017.

[29]   J. Fong, V. Crocher, Y. Tan, D. Oetomo, and I. Mareels, "EMU: A transparent 3D robotic manipulandum for upper-limb rehabilitation," *2017 International Conference on Rehabilitation Robotics (ICORR)*, pp. 771–776, Jul. 2017.

[30]   A. Akhoondi Asadi, "Design and Prototyping of a Pneumatically Enabled Haptic Device." M.S. Thesis, University of Manitoba, Manitoba, Canada, 2017

[31]   M.   Stride,   "Wrist   Movements,"   2018.   [Online].   Available: http://www.ergovancouver.net/wrist_movements.htm. [Accessed: July 20, 2020].

[32]   "Customizable Pneumatic Actuators, Dashpot & Snubber Experts - Airpot Corporation." [Online]. Available: http://airpot.com/. [Accessed: June 7, 2019].

[33]   "Airpel Double-Acting Universal Mount," *Customizable Pneumatic Actuators, Dashpot & Snubber Experts - Airpot Corporation*. [Online]. Available: http://airpot.com/product/airpel-double-acting-universal-mount-4/ [Accessed: Oct 6, 2019].

[34]   "SMC ITV0030-3ML-Q regulator, electro-pneumatic, IT/ITV0000/1000 E/P REGULATOR," *SMCpneumatics.com*. [Online]. Available: https://www.smcpneumatics.com/ITV0030-3ML-Q.html. [Accessed: Nov 6, 2019].

[35]   "SMC ITV1050-311S2 regulator, electro-pneumatic, IT/ITV0000/1000 E/P REGULATOR," *SMCpneumatics.com*. [Online]. Available: https://www.smcpneumatics.com/ITV1050-311S2.html. [Accessed: Nov 6, 2019].